Computer Networks 165 (2019) 106922

Contents lists available at ScienceDirect

Computer Networks

journal homepage: www.elsevier.com/locate/comnet

Density-aware cellular coverage control: Interference-based density estimation☆

Alperen Eroğlu[a,*], Okan Yaman[b], Ertan Onur[a]

[a] Department of Computer Engineering, METU, Ankara 06800, Turkey
[b] Department of Computer Engineering, İzmir Institute of Technology, 35430 İzmir, Turkey

ARTICLE INFO

Article history:
Received 9 May 2019
Revised 2 September 2019
Accepted 25 September 2019
Available online 26 September 2019

Keywords:
Cellular networks
Moving base stations
Base station density estimation
Density-adaptive networking
Network coverage

ABSTRACT

As demand for mobile communications increases, cells have to become smaller to efficiently use the scarce spectrum and to increase capacity, and small-cell networks will hereby emerge. They may be large in scale and highly dynamic resembling ad hoc networks due to the moving base stations. The variations in the density of the small cell networks impact the quality of service and introduce many novel challenges such as coverage control. We propose two novel base station density estimators, the interference-based density estimator (IDE) and the multi-access edge cloud-based density estimator (CDE) in a three-dimensional field. The estimators employ received signal strength measurements. We validate these two density estimators by using Monte-Carlo simulations. Furthermore, we analyze the impact of density on network outage in cellular networks and propose a density-aware cell zooming technique. According to the observations, base station (BS) density affects network coverage significantly. Received signal strength (RSS)-based density estimators can easily be implemented and applied in the network communication stack although they are more prone to shadowing and fading. Under favour of the density-aware cell zooming method, the network outage can be managed dynamically by adapting the transmit power, which provides a self-configurable and -organized network.

1. Introduction

A new trend for future networks is emerging along with the recent applications, innovations, and technologies in cellular networking. In order to meet the requirements of emerging applications for a larger capacity, cellular networks morph away from inflexible and centrally-managed infrastructures to large-scale collectives of small and mobile cells. Cellular networks equipped with mobile and nomadic base stations present a change in the characteristics of networks toward densified deployments of mobile base stations (BSs), incessantly changing topologies and dynamic infrastructures [1,2]. The dynamism in the infrastructure reflects itself as unpredictably base station density introducing some new challenges that have to be managed at run-time [3]. Most of the changes in the topology are not predictable in advance [4]. Hence, applications such as capacity planning, coverage control, interference management, energy conservation and quality of service provisioning have to be critically modified for efficient and proper operation by taking into consideration of future trends [1,2,5].

Density of base stations in future cellular networks, e.g., 5G networks, will vary in time and space because of mobile base stations (e.g., cell on wheels and unmanned aerial vehicles (UAVs)) [1,6], user-controlled base stations [7] (e.g., femtocells bought and controlled by end-users), green operation (e.g., sleep scheduling of base stations), and gradual deployment of base stations [8,9]. Resources in radio access, transport, and core networks will be wasted if related parameters are not adapted to the network density [10]. For instance, in Section 4, it is illustrated that any changes in the base station density affect the network parameters such as transmit power and network outage [11,12]. A decrease in the network density increases the outage probability. If the network is dense, the outage probability will then decrease with the same transmit power. For adapting the network to the changes in the density of base stations, robust network density estimators in a three-dimensional field are required [12,13]. We assert the third dimension considering drone base stations (cells on wings).

The need for energy-efficient dynamic networks presents the concept of cell zooming [14]. Cell zooming concept may include different schemes such as controlling the physical layer parameters like changing transmit power of the base stations, relying on

☆ This work is partially presented in 21st Conference on Innovation in Clouds, Internet and Networks (ICIN2018) held on February 19–22 in Paris, France.

* Corresponding author.
E-mail address: alperen@ceng.metu.edu.tr (A. Eroğlu).

https://doi.org/10.1016/j.comnet.2019.106922
1389-1286/

relaying, sleep scheduling of base stations, or employing multiple base stations [14,15]. Algorithms for cell zooming can be classified into static and dynamic algorithms. Considering the network density together with the transmit power is presented as a solution in the scope of cell zooming [12]. Adapting and optimizing the transmit power with the help of user equipment, reducing energy consumption without switching off base stations, determining the optimal height of the antenna of base stations, considering received signal strength (RSS) with a propagation model are presented as self-healing approaches under the concept of cell zooming [16,17]. In this study, we control the cell size dynamically with the help of a density-adaptive transmit power mechanism considering outage probability and effective density of moving base stations.

In this paper, we focus on the density estimators and network outage in order to adapt the transmit power of base stations for cell zooming. The contributions and structure of this paper can be summarized as follows:

- The first and foremost contribution of this paper is the interference-based density estimator presented in Section 2. Using an aggregate interference model, we propose a system design for density estimation of moving base stations in mobile networks in Section 2.2.1. Moreover, we propose multi-access edge cloud-based network density estimator (CDE) in a three-dimension field in Section 2.2.2 following the same approach employed in [18,19] which was developed for two-dimensional ad hoc networks. Most of the existing density estimators are operational only in two-dimensional Euclidean space. Satisfying the requirements for having a three-dimensional estimator in mobile networks is the gap this paper fills in. The interference-based density estimator (IDE) is modeled considering uniform randomly deployed a network of base stations. We validate the proposed estimator by Monte-Carlo simulations. The simulation results validate the model and show the accuracy of the proposed estimator is at an acceptable level in Section 3. We also discuss two density estimators by considering neighbor proximity indices, log-normal shadowing, path-loss models, and non-uniform distributions in Section 3.4.
- As the second contribution, we analyze the impact of network density on outage probability in cellular networks by employing a simple analytic model validated by simulation results in Section 4. A concise and simple analysis is the main difference of this contribution from other studies. We propose an analytic model for computing the outage probability based on base station density and validate it using Monte-Carlo simulations. Outage probability analysis in three dimensions is the novelty of the work. The results of this study assert that density-awareness in cellular networks is required to increase capacity and provide an efficient network. A novel outage model based on the density is introduced in Section 2.3, and the validation of this model is presented in Section 5.
- As the last contribution is founded on the first two, we propose a density-aware transmit power adaptation technique which makes a relation between the density of base stations, network outage, and transmit power. By using the proposed density estimator, moving or stationary base stations will be capable of adapting their transmit power in a distributed fashion. The results of this study assert that density awareness in cellular networks is required to increase the capacity and provide an efficient network. We will discuss how the transmit power is adapted based on network density in Section 2.4, and we demonstrate the verification results of the model in Section 6. Finally, Section 7 reviews categorically the existing studies which show the importance of base station density, network outage and transmit power as run-time adaptable and self-optimized parameters for self-organized future networks.

2. Density-aware coverage control

We assume that the density of base stations may change because of sleep scheduling for energy conservation, because of failures of base stations or because of cells on wheels or wings (mobile base stations) such as unmanned aerial vehicles (UAVs). A static configuration of network parameters under this assumption will waste resources and will not be practicable. A robust network density estimator for coverage control that adapts itself to the instant network density is required. In the sequel, we present two techniques for estimating the density of base stations in a three-dimensional Euclidean space. Then, we present the density-aware outage analysis and using this model we propose a density-aware transmit power adaptation technique for coverage control in cellular networks where the number of base stations varies in time and space.

2.1. System model

In an m-dimensional Euclidean space, we assume that a large number of nodes (base stations and UEs) are distributed uniform randomly [20,21]. It is assumed that the random variables indicated the number of nodes deployed in any disjoint Borel set A_1 and A_2 are independent and follow a Poisson distribution with a mean density λ nodes per unit m-volume. The derivation of the distance distribution to k^{th} nearest neighbor for any dimension in uniformly random networks is investigated clearly in [20]. Therefore, node positions form an m-dimensional homogeneous Poisson Point Process [20–22].

By taking one of the user equipment (UE) in the uniform randomly deployed cellular network as the reference node (receiver), let's denote the distance of the reference node to its k^{th} nearest neighbor r_k with the random variable $\mathbf{R_k}$. The PDF of $\mathbf{R_k}$ is

$$f_{\mathbf{R}_k}(r_k) = e^{-\lambda c_m {r_k}^m} \frac{m(\lambda c_m {r_k}^m)^k}{r\Gamma(k)}, \tag{1}$$

where $c_m {r_k}^m$ is the volume of the m-dimensional ball with radius r_k [22]. The coefficient c_m is defined as

$$c_m = \begin{cases} \frac{\pi^{\frac{m}{2}}}{(m/2)!}, & \text{for even m} \\ \frac{\pi^{\frac{m-1}{2}} 2^m (\frac{m-1}{2})!}{(m)!}, & \text{for odd m,} \end{cases} \tag{2}$$

where Γ is the gamma function interpolating the factorial function [23]. For example, $\Gamma(k)$ equals to $(k-1)!$. When $m = 1, 2$ or 3 V_m is 2, π and $4\pi/3$, respectively. For instance, a vehicular network on a road can be modeled in one dimensional space where $m = 1$ and $V_m {r_k}^m = 2r_k$ m. If it is in two dimensional, then $m = 2$ and $V_m {r_k}^m = \pi {r_k}^2$ m^2 are considered. Distribution of unmanned aerial vehicles in space may require a three dimensional model, where $m = 3$ and $V_m {r_k}^m = 4\pi {r_k}^3/3$ m^3.

We assume that a large number of base stations are deployed in a cellular network and the positions of BSs follow uniform random distribution in the three-dimensional Euclidean space with density λ (nodes/m^3). We exploit the simple path-loss model; the received signal power x_k of a BS from its k^{th} nearest neighbor that is r_k meters away is $x_k = CP_t \left(\frac{r_0}{r_k}\right)^{\gamma}$ where $\gamma \leq 3$ is the path-loss exponent, C accounts for the attenuation factor at a reference distance of r_0 meters and the impact of non-distance-related factors such as antenna gains, calculated by using $GtGr((300 \times 10^6/f)/(4\pi))^2$, where G_t is the transmitter receiver antenna gain in dB, G_r is the receiver antenna gain in dB, and (f) is the frequency with value of

2400×10^6 Hz. For simplicity we set $r_0 = 1$ m; then $x_k = CP_t r_k^{-\gamma}$. The transmit power of base stations is represented as P_t. The received signal strength with the random variable $\mathbf{P_k}$ is a function of $\mathbf{R_k}$. For the sake of generality, the probability density function of $\mathbf{P_k}$ calculated using above PDF of $\mathbf{R_k}$ and the simple path-loss model is:

$$F_{\mathbf{P}_k}(x_k) = \frac{m\lambda^k r_0^{mk-1} c_m^k \left(\frac{x_k}{CP_t}\right)^{k\left(\frac{1-m}{\gamma}\right)} e^{-\lambda c_m r_0^m \left(\frac{x_k}{CP_t}\right)^{\frac{-m}{\gamma}}}}{\Gamma(k)}. \tag{3}$$

Although we assume moving base stations, we suppose that the locations of base stations and user equipment do not change dramatically during the measurement period. The estimator can compute the estimate over a single slot that can be very short. Therefore, the network can be considered stationary throughout the estimation period. This system-level model is based on a generalization of Winner II channel models following a stochastic approach and statistical distribution, which can be used for indoor and outdoor scenarios [24]. Moreover, we assume that a dedicated control channel is only implemented by BSs, therefore the interference from UEs is not considered in this work. In a coordinated fashion, we assume that UEs can receive signals only its corresponded base stations.

2.2. Network density estimators

In this work, we concentrate only on the density of base stations that is called as network density; we do not deal with the density of users. The received signal strength (RSS) of signals transmitted by BSs and measured by a user equipment (UE) is highly correlated to the density of base stations. Therefore, we construct two techniques for estimating the network density using the RSS measurements of UEs. Firstly, we present a novel estimator that uses the aggregate interference from the nearest N base stations. This estimator is called as the interference-based density estimator. Secondly, we revert an early density estimator developed for two-dimensional ad hoc networks and adapt it to the mobile networks where multi-access edge cloud computing (MEC) is employed. Hence, we call it the MEC-based density estimator.

2.2.1. Interference-based network density estimator (IDE)

By selecting a random position as the location of a reference UE, let's denote the distance of the UE to the k^{th} nearest base station r_k with the random variable $\mathbf{R_k}$. Based on the system model presented in Section 2.1, the joint probability density function (PDF) of the distances of the randomly selected reference point to the first N BSs, $\mathbf{r} = (r_1, r_2, \ldots r_N)$ denoted with the random variables $\mathbf{R} = (R_1, R_2, \ldots, R_N)$ as derived from [21] is

$$f_{\mathbf{R}}(\mathbf{r}) = e^{-\frac{4}{3}\pi\lambda r_N^3} (4\pi\lambda)^N r_1^2 \ldots r_N^2 \, d\mathbf{r},$$

Assume that all these N base stations transmit a signal at the same time. The expected value of the aggregated interference measured by a UE located at a random point then becomes

$$\begin{aligned}\mu_I &= \int_0^{\infty} \int_0^{r_N} \ldots \int_0^{r_2} \sum_{i=1}^{N} CP_t r_i^{-\gamma} f_{\mathbf{R}}(\mathbf{r}) d\mathbf{r} \\ &= \frac{3CP_t (4/3\pi\lambda)^{\gamma/3} \Gamma(N - \gamma/3 + 1)}{(3-\gamma)\Gamma(N)},\end{aligned} \tag{4}$$

where $\Gamma(.)$ is the gamma function, and $\gamma < 3$.

In the Interference-based Density Estimator method, each UE measures the aggregate interference from the nearest base stations and report these measurements to their associated base stations. In the coverage of each base station, there will usually be a large number of UEs, say M. The base station will average the aggregate interference measurements of UEs and then will estimate the network density as

$$\widehat{\lambda}_{\text{IDE}} = \frac{1}{4\pi} \left(\frac{\overline{\mu}_I (3-\gamma)\Gamma(N)}{3^{1-\gamma/3} CP_t \Gamma(1 + N - \gamma/3)} \right)^{3/\gamma}, \tag{5}$$

where $\overline{\mu}$ is the average of aggregate interference measurements by M UEs. In IDE, all base stations can estimate the network density in a local fashion with the assistance of the UEs in their coverage areas. One can enhance the performance of $\widehat{\lambda}_{\text{IDE}}$ by averaging the individual estimates of base stations. Although, we call it interference, BS generates collision of signals intentionally to let UEs take samples.

2.2.2. Multi-access edge cloud based network density estimator (CDE)

We present the multi-access edge cloud-based density estimator (CDE) as the second estimator model. In CDE, we assume that user equipment measures the received signal strength (RSS) of pilot signals transmitted by base stations at various non-overlapping time slots and send these measurements back to their associated base stations. Then, the base stations convey these measurements to a multi-access edge computing (MEC) entity. Afterwards, the MEC employs these measurements to estimate the network density. We modify the two-dimensional model proposed in [19] to fit it into the three-dimensional Euclidean space. In this section, we present the theoretic basis of the maximum likelihood density estimator $\widehat{\lambda}_{\text{CDE}}$ where the actual density is λ in nodes/m^3.

By selecting a random position as the location of a reference UE let's denote the distance of the UE to the k^{th} nearest base station r_k with the random variable $\mathbf{R_k}$. The PDF of $\mathbf{R_k}$ [19] is

$$f_{\mathbf{R_k}}(r_k) = e^{-\frac{4}{3}\pi\lambda r_k^3} \frac{3(\frac{4}{3}\pi\lambda r_k^3)^k}{r_k \Gamma(k)}. \tag{6}$$

We represent the received signal power from the k^{th} base station x_k with the random variable $\mathbf{P_k}$ which is a function of $\mathbf{R_k}$ considering the system model presented in Section 2.1. Then, the cumulative distribution function (CDF) of $\mathbf{P_k}$ [19] becomes

$$F_{\mathbf{P}_k}(x_k) = \frac{\Gamma\left(k, \frac{4}{3}\pi\lambda x_k^{-3/\gamma} \left(\frac{1}{CP_t}\right)^{-3/\gamma}\right)}{\Gamma(k)}, \tag{7}$$

where $\Gamma(a, z) = \int_z^{\infty} t^{a-1} e^{-t}\, dt$ is the incomplete gamma function [19], when we consider the model for three-dimensional deployment of base stations and user equipment.

Let x_i denotes the RSS of a pilot signal transmitted to a UE by its k_i^{th} nearest base station, and (7) is the CDF of x_i. After n RSS samples $x_1, x_2, \ldots, x_n$ and the corresponding neighbor proximity indexes $k_1, k_2, \ldots, k_n$ are collected by UEs collectively *from non-overlapping regions*, UEs convey these measurements to the MEC over base stations. Then, the MEC can compute the maximum likelihood estimator, $\widehat{\lambda}$. We assume the node distribution of base stations in the $m-$dimensional space follows a homogeneous Poisson point process (PPP); and the RSS measurements are independent since they are collected from non-overlapping regions. The maximum likelihood density estimator becomes as in [12,19]

$$\widehat{\lambda}_{\text{CDE}} = \frac{K-1}{\frac{4}{3}\pi \sum_{j=1}^{n} \left(\frac{x_j}{P_t C}\right)^{-3/\gamma}}, \tag{8}$$

where $K = \sum_{j=1}^{n} k_j$. The unit of density is nodes/m^3. $\widehat{\lambda}_{\text{CDE}}$ is an unbiased estimator and its variance goes to zero as more and more samples are collected from the field. Therefore, the number of collected samples impact K which in turn significantly impacts the accuracy of the estimator $\widehat{\lambda}$. It can be seen that the different dimensions have different c_m and m values [19,20]. Then, we can generalize the estimator as follows:

$$\widehat{\lambda}_{\text{CDE}} = \frac{K-1}{c_m \sum_{j=1}^{n} \left(\frac{x_j}{P_t C}\right)^{-m/\gamma}}.$$

2.3. Outage probability based on network density

By considering the PDF of $\mathbf{R_k}$ (6) and the CDF of $\mathbf{P_k}$ (7), we present the outage probability as the probability (P_O) of the received power of the signals transmitted by the closest base station (i.e., $k = 1$) and measured by the randomly located reference user being below the receiver sensitivity, T. Based on this definition, the outage probability becomes

$$P_O(\lambda) = F_{\mathbf{P}_{l_1}}(T) = e^{-4/3\pi\lambda(CP_t/T)^{3/\gamma}}, \tag{9}$$

where T is the receiver sensitivity (threshold) that is the minimum required received signal strength to intelligibly decode the signals [25]. (9) is different from its two-dimensional representation proposed in [26]. The dimension of the solution changes the network outage model. This network outage model analytically indicates that the outage probability and the base station density are two important interactive parameters. The network outage is also influenced by the path-loss exponent, transmit power of base stations and the minimum power requirement which is the threshold value as experimentally demonstrated in Section 4. The PDF decreases with $e^{-(CP_t/T)^{3/\gamma}}$ when P_t increases, the outage probability becomes zero. When T increases the expected value will be 1. The PDF of received signal strength (3) will affect the outage probability. If P_t increases the received signal strength will increases, which means more and more UEs can receive the signal with a higher RSS. In this formulation, we suppose that there is a robust interference cancellation technique implemented in the system. That is why we consider only the received signal strength instead of signal-to-interference-plus-noise ratio (SINR) [12].

2.4. Density-aware cell zooming

Let's assume that the base stations located in a cellular network has an ability to estimate the network density. Then the adaptation of their transmit power levels using (9) would be possible in order to satisfy a provided outage probability level in a decentralized or distributed fashion [12]. Using (9), the transmit power has to be adapted to its minimized value

$$P_t^* \geqslant \frac{T}{C}\left(-\frac{3\log\left(P_O^*\right)}{4\pi\widehat{\lambda}}\right)^{\gamma/3}, \tag{10}$$

where the required outage probability P_O^* is a network design parameter set by the network operator and $\widehat{\lambda}$ is either IDE or CDE. We assume that using some technique, IDE or CDE, base stations estimate the density of the network. Then, they employ the estimated density $\widehat{\lambda}$ to set their transmit power using (10).

Although many phenomenon and impairments that affect the received signal strength are not included, this model is very practical as a result of its simplicity. Many users in a cell may independently measure the received signal strength. These measurements may be transmitted to a mobile edge computing (MEC) entity, and fusion of the results may be exploited by the MEC and base stations to decrease the impact of fading and shadowing. By means of the user equipment signal strength measurements, base stations will be able to arrange their transmit powers immediately bounded with the time period of the density estimation. A simple and fast density estimator will be very rewarding for this matter. Hence, we suggest two novel three-dimensional density estimators.

All these models need to be validated. In the sequel, we validate these models by using Monte Carlo simulations and leverage them to demonstrate their applications and analyze the outcomes for different scenarios.

3. Validation of network density estimators

In this section, we present the simulation results for validating IDE and CDE. Besides, we discuss these two estimators based on some analyses including the impact of neighbor proximity indices, log-normal shadowing, path-loss models, and different non-uniform deployments.

3.1. Simulator design

These network density estimators are validated by Monte-Carlo simulations implemented using Matlab. In the simulations, a number of base stations and UEs are uniform randomly deployed in a three-dimensional Poisson process in Matlab. For each run of the simulator, the locations of BSs and UEs change randomly. We assume that UEs can measure the RSS from their closest base stations. Table 1 presents a summary of symbols and the parameters which are considered during the validations of two estimators. Actual density, λ, is the deployment density, which is the number of UEs and BSs divided by the volume (m^3). The estimated (effective) density, $\widehat{\lambda}$, is the computed density value after applying one of the density estimators in a network. Sparse deployment, λ_S, dense deployment, λ_D, ultra-dense deployment, λ_U show different deployment density for different network scenarios [12]. Path-loss exponent, γ, is the coefficient for the path-loss model in the range between 0 and 7, which is already determined as empirical values for different indoor and outdoor scenarios [18]. r_0 is the reference distance in the far-field of the antenna, which is selected as 1 m for simplicity. We assume that the random distances in the network are generally larger than the reference distance. P_t

Table 1
The symbols, notations, values and units of the 3-D simulation parameters.

Parameter	Default value	Units	Ref
Actual density, λ	[0.0001,0.003]	nodes/m^3	[12]
Estimated (effective) density, $\widehat{\lambda}$	(5) or (8)	nodes/m^3	
Sparse deployment, λ_S	0.0005	nodes/m^3	[12]
Dense deployment, λ_D	0.0015	nodes/m^3	[12]
Ultra-dense deployment, λ_U	0.003	nodes/m^3	[12]
Path-loss exp. γ	$0 \leq \gamma \leq 7$		[24]
Reference distance, r_0,	1	m	[19]
Transmit power, P_t	[10,100]	mW	[27]
Adapted transmit power, P_t^*	(10)	mW	
Threshold (Receiver sensitivity), T	5×10^{-13}	mW	[12]
Required outage probability, P_O^*	[0,1]		[12]
Simulated outage probability, P_O	[0,1]		[12]
Analytic outage probability, P_{O_A}	[0,1]		[12]
Nearest neighbor index, k	[1,∞)		[12]
Selected maximum value of nearest neighbor index, N	[1,∞)		[12]
C	10^{-5}		[12]

is the transmit power for base stations which is selected up to the 20 dbm considering the small cell requirements [12]. P_t^* is the transmit power for base stations adapted by the proposed model (10). T is calculated by $T = CP_t r_c^{\gamma}$, where r_c is the maximum communication range. This threshold value for the network outage model, which is the receiver sensitivity, and it provides the minimum power requirement to receive a signal [12]. P_O^* is the required outage probability which is provided by the network operator. P_O is simulated and calculated by performing the proposed model (9). P_{O_A} is calculated by using the CDF of the network outage model (7). The nearest base station neighbor for a UE is represented as k which is in range of $[1,\infty)$ for a model based on Poisson Point Process. N is the selected maximum value of the nearest base station index. Moreover, C is a constant originated from non-distance-based factors and antenna gain, which is calculated as explained in Section 2.1. The results are the averages of 10^4 runs.

3.2. Validation of the interference-based network density estimator (IDE)

To validate IDE, base stations are assumed to be randomly deployed with various densities from sparse networks to dense networks in a spherical simulation environment with a radius of 250 m. A randomly selected point designates the location of a UE. We assume that this UE measures the aggregate signal power from the first six base stations closest to it; $N = 6$. The averages of 10^4 simulation runs are compared to the results of the analytic model (4) presented in Section 2 under the same set of parameter values.

Fig. 1 shows the simulation and analytic results based on different path-loss exponent (γ) values and various densities. As can be seen in Fig. 1, the simulation results validate μ_I in (4). The accuracy of the results decreases as the environment gets harsher, i.e., when path-loss exponent becomes larger. In harsh environments with a large γ, only the overall strength of the signals become smaller. The errors in the channel model such as deviations in the γ estimates will significantly impact the density estimators.

We define the average absolute percentage deviation as AAPD $= 100|\widehat{\lambda} - \lambda|/\lambda$. We present the AAPD results for IDE ($\widehat{\lambda}_{\text{IDE}}$) in Table 2. For various deployments with different densities, the AAPD results show that the estimation results are at an acceptable level; the AAPD values are generally less than 3%. IDE considers only path loss and non-distance related fading in signal measurements. Over channels that are prone to different types of fading, the deviations will be larger.

3.3. Validation of the multi-access edge cloud-based network density estimator (CDE)

In the simulations for validating the Multi-acces Edge Cloud-based Network Density Estimator (CDE), a set of user equipment and base stations are assumed to be uniform randomly deployed in a field of interest following 3-D Poisson process in Matlab. At each run of the simulator, the locations change randomly. UEs measure the RSS from their first closest base stations by using the channel model described in Section 2.1 and these measurements are assumed to be collected at a mobile edge computing (MEC) entity. Therefore, $k_j = 1$ and $K = \sum_{j=1}^{n} k_j = n$, for $\widehat{\lambda}_1$ where n is the number of samples collated at the MEC. Then, (8) is employed to compute the estimator in nodes/m^3. The results are the averages of 10^4 runs. The values of the parameters employed in the simulations are shown in Table 1.

We present how accurate CDE performs in Table 3 for various actual deployment densities λ. The first column of this table is the actual density and the second column is the result of the estimator $\widehat{\lambda}$. CDE works with acceptable accuracy and the AAPD is always less than 3%.

The CDE results when $\lambda = 5 \times 10^{-4}$ nodes/m^3 for different path-loss exponent (γ) values are shown in Table 4. The AAPD values are considerably small for any channel model with various path-loss exponent values. The effect of the path-loss exponent on the accuracy of the CDE is not dramatic.

Unfortunately, CDE has some deficiencies. Firstly, similar to IDE it only considers the path-loss and the non-distance related fading. Secondly, the time to compute CDE can be long. UEs collect measurements and send them back to the base stations. Base stations convey these measurements to the mobile edge computing (MEC) entity in the network and the MEC estimates the density and informs the base stations about the result. As the third deficiency, we can partially say that CDE may yield biased results when the measurements are collected from overlapping regions. Since we employ likelihood estimation, CDE depends on the strict assumption of independence among measurements. When the measurements are collected from overlapping regions, there will be a large amount of correlation among measurement samples that will create a bias in the estimates.

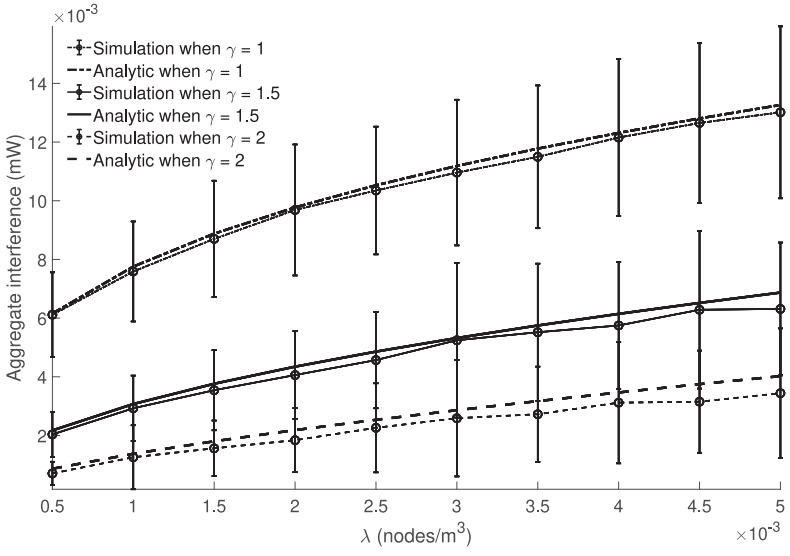

Fig. 1. Mean aggregate interference power (mW) for various deployment densities when $\gamma = 1, 1.5$ and 2, respectively, and $P_t = 100$ mW.

Table 2
The AAPD and 99% confidence limits in the estimator for various deployments (λ) **(nodes/m^3)** where $\gamma = 1.5$ and $N = 6$.

$\lambda(\times 10^{-3})$	$\widehat{\lambda}_{\text{IDE}}(\times 10^{-3})$	AAPD (%)	99% confidence limits of $\widehat{\lambda}_{IDE} \times (10^{-6})$
0.2	0.20	0.81	± 0.17
0.4	0.40	0.06	± 0.36
0.6	0.60	0.73	± 0.57
0.8	0.81	1.39	± 0.84
1	1.03	2.52	± 1.16
1.2	1.19	0.63	± 1.01
1.4	1.43	1.91	± 1.55
1.6	1.82	0.65	± 1.48

Table 3
The AAPD in CDE for various actual deployment densities λ **(nodes/m^3)** where $\gamma = 3$, and $\widehat{\lambda}_{CDE_1}$ **(nodes/m^3)**.

$\lambda(\times 10^{-3})$	$\widehat{\lambda}_{CDE_1}$ $(\times 10^{-3})$	AAPD (%)	99% confidence limits of $\widehat{\lambda}_{CDE_1}$ $(\times 10^{-5})$
1	0.98	2.50	± 0.80
2	1.96	2.09	± 1.54
3	2.92	2.66	± 2.37
4	3.91	2.16	± 3.18
5	4.93	1.44	± 4.06
6	5.93	1.16	± 4.73
7	6.85	2.11	± 5.66
8	7.91	1.12	± 6.49

Table 4
The impact of the path-loss exponent (γ) on the CDE and the AAPD in the estimators where the actual deployment density is $\lambda = 5 \times 10^{-3}$ (nodes/m^3), and $\widehat{\lambda}_{CDE_1}$ (nodes/m^3).

γ	$\widehat{\lambda}_{CDE_1}$ $(\times 10^{-3})$	AAPD (%)	99% confidence limits of $\widehat{\lambda}_{CDE_1}$ $\times (10^{-5})$
2	4.91	1.71	± 3.54
2.5	4.90	1.94	± 3.46
3	4.93	1.32	± 3.55
3.5	4.91	1.87	± 3.54
4	4.92	1.52	± 3.54
4.5	4.94	1.29	± 3.57
5	4.90	1.98	± 3.54
5.5	4.91	1.75	± 3.44
6	4.93	1.45	± 3.50

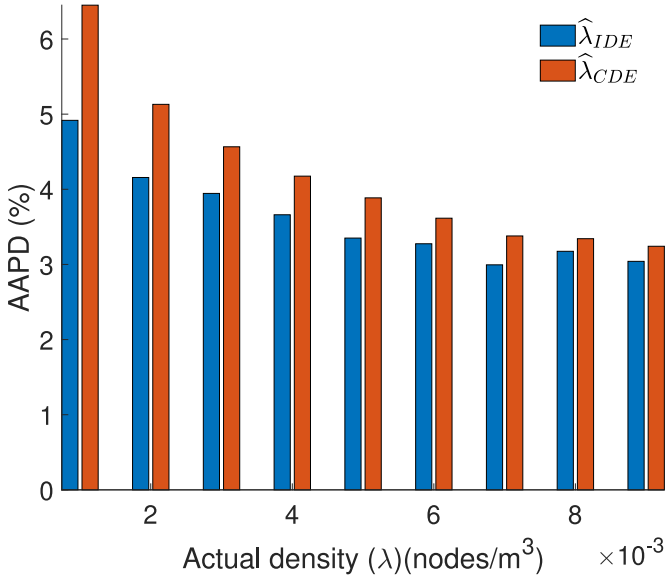

Fig. 2. The accuracy of different estimation, average absolute percentage deviation (AAPD) results of $\widehat{\lambda}_{IDE}$ and $\widehat{\lambda}_{CDE}$, respectively (nodes/m^3) when $\gamma = 1.5$.

3.4. Discussions about density estimators

With the help of the Monte Carlo simulations, two different approaches are performed by using both 3-D edge cloud-based density estimator and the newly proposed 3-D aggregate interference based density estimator. In these experiments, we assume that UEs are able to collect RSS measurements from their first six ($k = 1, 2, 3, 4, 5, 6$) and ($N = 6$) closest BSs. As it can be seen in Fig. 2 and Table 5, the aggregate interference method provides more accurate results in comparison to the collaborative estimator. In these simulations at each run nodes positions are changed randomly.

When both of two estimators use the first k^{th} closest BS measurements, the results are really prone to the accuracy of the RSS measurements. In addition to the number of proximity indexes, the location of base stations and UEs that RSS values collected also affect the accuracy of the estimators. In interference-based density estimator, if the RSS measurements are collected from a large number of distant base stations, the estimations provide more accurate results. The aggregate interference-based estimator can be performed by an individual node, however, CDE requires the other nodes' contributions to provide more accuracy. The MEC-based density estimator can be performed even when the channel conditions are very harsh such as when the path-loss exponent is greater than the value of three.

3.4.1. Impact of neighbor proximity indices

We simulate an environment which is a spherical volume as can be seen in Fig. 3. In this volume, we distribute the base stations and user equipment uniform randomly. In this case, as a different application scenario from Section 3.3, all of the user equipment is involved in the estimation process in a fixed topology. At each step, UEs collect RSS measurements from the closest BS for computing $\widehat{\lambda}_{CDE_1}$ in the first variant of CDE. In the second variant of CDE, UEs collect RSS measurements from the first six closest base stations for computing $\widehat{\lambda}_{CDE_6}$. We assume that each UE sends these measurements to MEC over the associated BS. Then, MEC performs (8) by using these measurements. The results are presented in Table 6.

According to the results, CDE has accurate outcomes. However, if we increase the number of closest neighbor BSs to get RSS

Table 5
The accuracy of different estimation AAPD results of $\widehat{\lambda}_{IDE}$ **(nodes/m^3)**, and $\widehat{\lambda}_{CDE}$ **(nodes/m^3)**, respectively when $\gamma = 1.5$.

λ ($\times 10^{-3}$)	$\widehat{\lambda}_{IDE}$			$\widehat{\lambda}_{CDE}$		
	$\widehat{\lambda}_{IDE}$, ($\times 10^{-3}$)	AAPD,%	99% confidence limits, ($\times 10^{-5}$)	$\widehat{\lambda}_{CDE}$, ($\times 10^{-3}$)	AAPD,%	99% confidence limits, ($\times 10^{-5}$)
1	0.95	4.92	$\pm$0.23	0.94	6.45	$\pm$0.20
2	1.92	4.16	$\pm$0.46	1.90	5.13	$\pm$0.39
3	2.88	3.95	$\pm$0.69	2.86	4.57	$\pm$0.57
4	3.85	3.66	$\pm$0.94	3.83	4.17	$\pm$0.74
5	4.83	3.35	$\pm$1.13	4.81	3.89	$\pm$0.94
6	5.80	3.28	$\pm$1.42	5.78	3.62	$\pm$1.15
7	6.79	2.99	$\pm$1.59	6.76	3.38	$\pm$1.29
8	7.75	3.17	$\pm$1.87	7.73	3.34	$\pm$1.45

Table 6
The actual densities (λ) (nodes/m^3) versus the estimated densities ($\widehat{\lambda}$) (nodes/m^3) for $\widehat{\lambda}_{CDE_1}$ and $\widehat{\lambda}_{CDE_6}$. The AAPD (%) results are also presented.

λ ($\times 10^{-3}$)	$\widehat{\lambda}_{CDE_1}$			$\widehat{\lambda}_{CDE_6}$		
	$\widehat{\lambda}_{CDE_1}$, ($\times 10^{-3}$)	AAPD,%	99% confidence limits, ($\times 10^{-6}$)	$\widehat{\lambda}_{CDE_6}$, ($\times 10^{-3}$)	AAPD,%	99% confidence limits, ($\times 10^{-6}$)
1	0.94	6.43	$\pm$1.84	0.91	9.18	$\pm$0.89
2	1.89	5.28	$\pm$2.73	1.85	7.41	$\pm$1.33
3	2.86	4.59	$\pm$3.16	2.81	6.48	$\pm$1.69
4	3.83	4.21	$\pm$3.76	3.76	5.88	$\pm$1.82
5	4.80	3.96	$\pm$4.31	4.72	5.51	$\pm$2.12
6	5.78	3.59	$\pm$4.67	5.69	5.15	$\pm$2.32
7	6.76	3.46	$\pm$5.09	6.66	4.91	$\pm$2.40
8	7.73	3.34	$\pm$5.44	7.62	4.73	$\pm$2.59

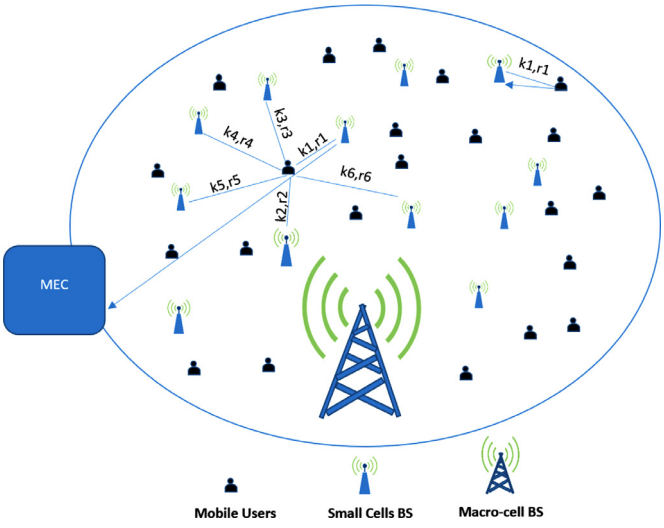

Fig. 3. Collecting RSS measurements from the k^{th} nearest BS.

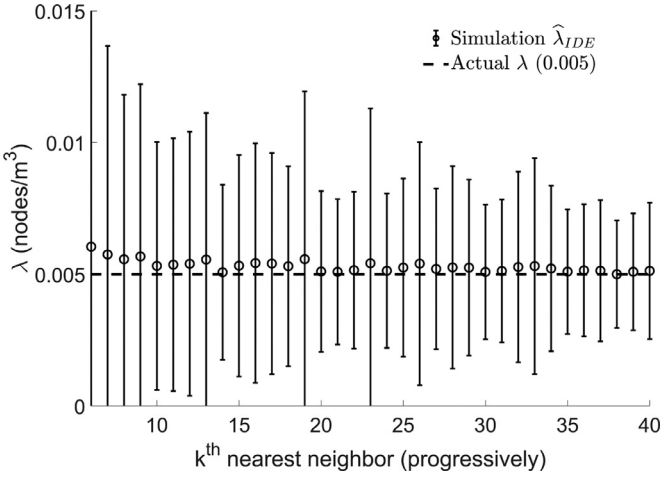

Fig. 4. The estimator $\widehat{\lambda}_{IDE}$ results along with different proximity indexes k where $\gamma = 3$, and $\lambda = 0.005$ (nodes/m^3).

measurements, it increases the sampling from overlapping regions, which results in less accurate outcomes than the estimation results including RSS measurements from the first closest BS. An increase in the number of the nodes near the network edge effects the results negatively since measurements are exposed to the shadowing and the multi-path fading more than the nodes near the middle of the network. Moreover, Table 6 shows that when the number of closest neighbors increases the variance of the estimator results declines.

The neighbor proximity has also impact on IDE, which is presented in Fig. 4. It can be seen that when the proximity index increases, the accuracy of the estimator improves, and the variance of the results decreases.

3.4.2. Impact of log-normal shadowing

In order to derive our proposed density estimators, we exploit the deterministic simple path-loss model as presented in Section 2.1. However, due to the obstructions such as buildings, walls, or trees, received signal strength measurements are subject to a stochastic channel impediment which is called shadowing. These stochastic external factors give rise to log-normally distributed (or normally distributed in the dB scale) received signal strength results. Although two proposed estimators consider small-scale fading effects within the coefficient C as expressed in Section 2.1, shadowing is not incorporated in these models. For this reason, a set of simulation is conducted by using (11) to analyze the shadowing effects:

$$P_k(r_k) = 10\left(\log_{10}(C) + \log_{10}(P_t) + \gamma \log_{10}\left(\frac{r_0}{r_k}\right)\right) + \psi\sigma_\psi \qquad (11)$$

where ψ is based on zero-mean Gaussian distribution with a standard deviation of σ_ψ. We analyze the impact of log-normal shadowing characterized by the standard deviation of $2 \leq \sigma_\psi \leq 12$ dB on both proposed estimators [28]. From these results, we observe that while the effect of shadowing increases, the accuracy of the results significantly decreases. Thus, the proposed estimators can be enhanced by incorporating shadowing models. To remove

shadowing, we apply (12) a different path-loss model which is already presented in [29].

$$P_k(r_k) = CP_t\left(\frac{r_0}{r_k}\right)^{\gamma} e^{-\frac{\sigma^2}{2\left(\frac{10}{\log(10)}\right)^2\gamma^2}}, \tag{12}$$

where σ represents the standard deviation of the log-normally distributed shadowing and can be computed by collecting multiple x_i values between the same pair of nodes. When the standard deviation is 2 dB, 3 dB, and 4 dB, the AADP results of estimations obtained from IDE are 3.27%, 24.75%, and 62.26%, respectively. However, if we incorporate the shadowing model, and leverage (12) instead of simple path-loss model, the AADP results are equal to 0.76% and 13.93%, and 38.07%, respectively. Since the cooperative density estimator has cooperation among the nodes, the results of this estimator may be less prone to shadowing effects than the interference-based density estimator. By considering our observations and another analysis for RSS-based distance estimation under log-normal shadowing [30], it can be concluded that RSS-based estimators are highly susceptible to log-normal shadowing even when a shadowing model is applied. The main observation from the impact of shadowing analysis is that log-normal shadowing corrupts estimations and causes exponentially growing errors over the measurements.

3.4.3. Impact of path-loss model

Choosing a path-loss model in wireless networks is critical if an RSS-based method is using. For the sake of simplicity, the simple path-loss model which is considered as an isotropic model can be chosen while deriving the analytic models as we do in this paper. However, we can enhance our models to overcome the line-of-sight and non-line-of-sight effects at the same time in a wireless network. Thus, we leverage an anisotropic path-loss exponent which is already introduced in [31], and demonstrate the results by comparing these two different approaches. $\beta = -\frac{log\frac{P_{min}}{P_t}}{log(R_{max})}$ is the anisotropic path-loss coefficient [31], where R_{max} is the distance between a BS and the farthest position of the coverage area, P_{min} is minimum threshold power in this coverage boundary. Fig. 5a and b present the results from IDE and CDE when different coverage areas (R) are considered. Since CDE pushes for collaboration among the nodes, and take samples from different parts of the network, CDE has more accurate results than IDE. While the size of the network area is changing, the accuracy of the anisotropic model is higher than the isotropic one. If we use the isotropic path-loss coefficient, since it is a constant value which we choose at the beginning, it does not change during the estimation process. However, the anisotropic model can adapt itself to these changes at run-time, and provide more convenient values to the estimators.

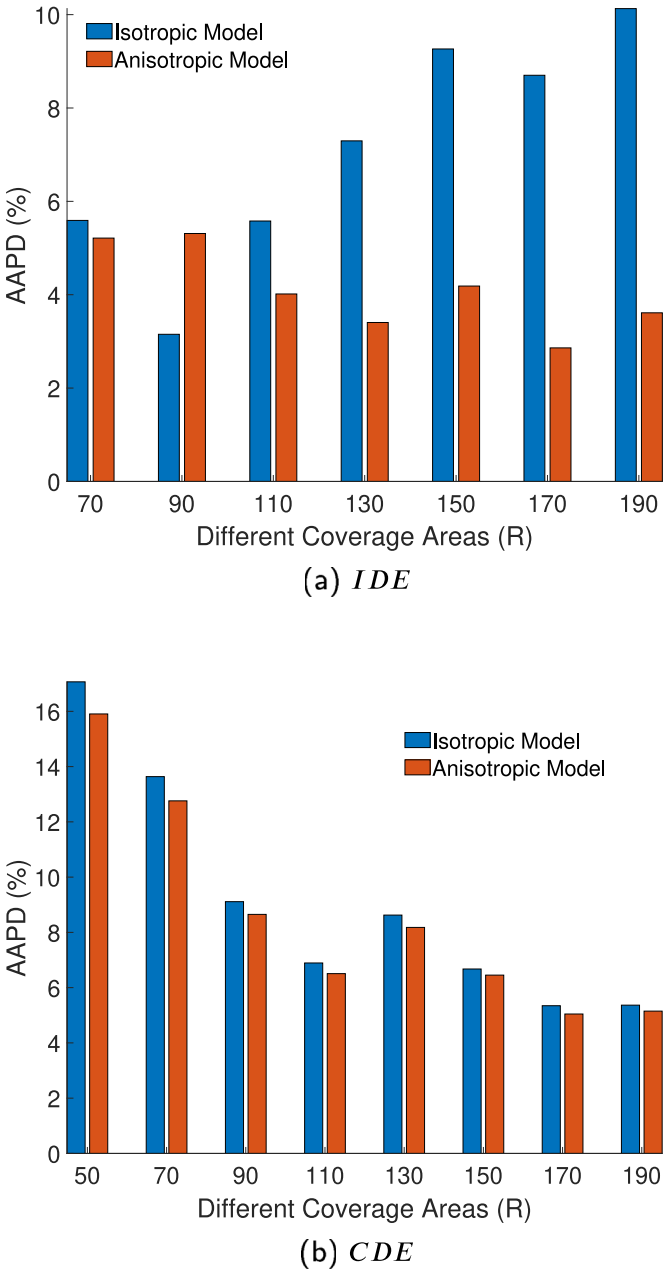

Fig. 5. The comparison of isotropic and anisotropic path-loss model for different estimations, and average absolute percentage deviation (AAPD) results of $\widehat{\lambda}_{IDE}$ and $\widehat{\lambda}_{CDE}$, respectively when isotropic $\gamma = 2$.

3.4.4. Impact of non-uniform distributions

Since the cellular networks have a stochastic nature in real-life, the distribution of base stations and users may be non-uniform. In this study, although we assume that distributions of BSs and UEs are uniform to propose a tractable and easily understandable analytic model, we also analyze some non-uniform deployments to show how this phenomenon affects our proposed estimators. To create non-uniform scenarios, we exploit Beta (B) distribution which is an asymmetrical two-parameter distribution close to the log-normal distribution [32]. (13) represents the PDF of Beta distribution [33]. Based on different shape tendencies provided by B distribution, we deploy BSs and UEs in a 3-D simulation environment. Table 7 roughly categorizes all these different deployments into six scenarios entitling different tendencies. In the first four scenarios, we deploy BSs and UEs based on B distribution by using the values of a and b for each of BS and UE distributions. In the last two remaining scenarios, firstly we uniformly deploy BSs, but we apply a and b values in Table 7 for the distribution of UE, which are following the three non-uniform tendencies. Secondly, we just use these two parameters for the BS distribution, but the deployment of UEs are selected uniformly. In Fig. 6, all these tendencies employing different values of a and b are demonstrated. In Table 7, the first scenario is called *Uniform* since the parameters a and b of B distribution are equal to 1, where BSs and UEs are located uniformly in the environment. The second one is called *Central Tendency* providing a centralized distribution so that BSs and UEs are gathered at the center of the spherical network area as indicated in Fig. 6. *Centrifugal Tendency* is the third scenario where the distributions of BSs and UEs are off-centered. This tendency locates BSs and UEs close to the boundaries of the network. The tendency of *Skewness* has a skewed shape, in which UEs and BSs are located

Table 7
When the actual density value equals to $1(\times 10^{-4})$ (λ) (nodes/m^3), estimated density results ($\widehat{\lambda}$) (nodes/m^3) of $\widehat{\lambda}_{IDE}$ and $\widehat{\lambda}_{CDE}$ for different uniform and non-uniform distributions are presented. All AAPD (%) results are also presented with their 99% confidence interval ($CI_{99\%}$).

Distributions		Shape parameters		$\widehat{\lambda}_{IDE}$			$\widehat{\lambda}_{CDE}$		
BS	UE	a	b	$\widehat{\lambda}_{IDE}$ $(\times 10^{-4})$	AAPD %	$CI_{99\%}$ $(\times 10^{-6})$	$\widehat{\lambda}_{CDE}$ $(\times 10^{-4})$	AAPD %	$CI_{99\%}$ $(\times 10^{-6})$
Uniform	**Uniform**	1	1	0.98	1.24	±0.33	0.99	0.32	±0.40
Central	**Central**	3	3	0.65	34.84	±1.91	0.85	15.32	±0.74
Tendency	**Tendency**	5	5	0.85	14.86	±3.65	1.13	13.03	±1.43
		7	7	1.08	7.58	±3.08	1.50	49.58	±2.23
Centrifugal	**Centrifugal**	0.1	0.1	0.75	25.46	±2.35	1.74	74.00	±3.87
Tendency	**Tendency**	0.5	0.5	0.56	44.46	±2.24	0.63	37.30	±0.57
		0.7	0.7	0.48	52.45	±1.64	0.59	41.50	±0.43
Skewness	**Skewness**	1	3	1.11	10.70	±4.10	1.84	83.56	±2.38
Tendency	**Tendency**								
		4	1	0.77	22.78	±2.80	0.79	21.13	±1.09
Uniform	**Non-uniform**	10	10	0.71	29.01	±5.84	0.72	27.85	±0.26
		0.3	0.3	0.71	28.93	±8.43	0.53	46.89	±0.19
		0.5	0.5	0.73	26.86	±7.55	0.61	39.44	±0.22
		0.7	0.7	0.73	27.16	±7.03	0.65	34.94	±0.21
		1	4	0.94	6.26	±6.10	0.60	40.43	±0.32
		1	5	0.90	10.24	±5.77	0.56	44.35	±0.30
		4	1	0.51	48.77	±6.91	0.49	50.97	±0.21
		20	1	0.47	53.43	±4.23	0.38	61.62	±0.21
		20	10	0.61	38.90	±5.49	0.58	42.45	±0.26
		10	20	0.88	12.12	±6.11	0.81	19.06	±0.31
		100	20	0.55	45.40	±6.21	0.45	55.13	±0.23
Non-uniform	**Uniform**	1	20	0.52	47.86	±1.60	0.29	70.73	±0.28
		20	1	0.09	91.30	±1.86	0.32	67.65	±0.18

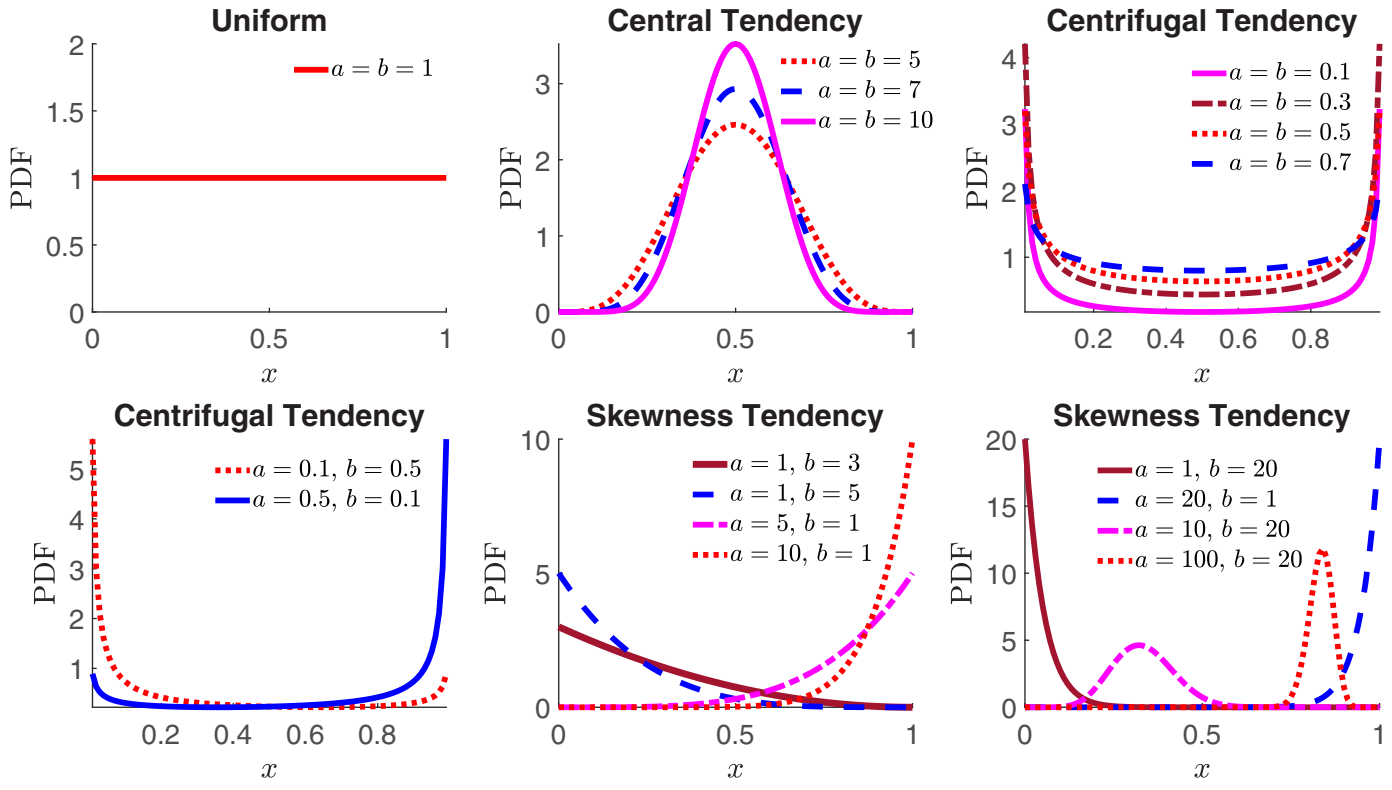

Fig. 6. The Probability Density Function (PDF) of B Distribution vs. x parameter when different a and b parameters are used.

at a particular region of the network. The last scenarios include *Non-uniform* distribution for UEs, and *Uniform* distribution for BSs, *Uniform* distribution for UEs, and *Non-uniform* distribution for BSs.

$$f(x|a,b) = \frac{1}{B(a,b)} x^{a-1}(1-x)^{b-1} I_{[0,1]}(x), \tag{13}$$

where $B()$ is the Beta function, a and b are two different shape parameters which change the shape of the distribution, and $I_{[0,1]}$ is to ensure that the values of the variable x is in the range of between 0 and 1.

According to our observations, we can state that the *Uniform Tendency* scenario where both BSs and UEs are deployed uniformly, the accuracy of the estimators are the best in comparison to the other cases as expected since we create our models based on the 3-D Poisson Point Process with an assumption including a uniform deployment of BSs and UEs.

In *Central Tendency*, while the level of the centrality is soaring IDE provides resilient results. The reason for this case is that when nodes (UEs and BSs) are close to each other near to the center of the environment, the amount of the path-loss, shadowing, the nodes causing non-negative effects at the corner of the network decrease. However, since CDE take samples from different UEs collaboratively, the closest nodes at the center cause an increase of overlapping measurements, and some sparse nodes near to the boundary of the network may not provide good measurements that are why CDE gives worsening outcomes as the central tendency is rising.

In scenarios built upon *Centrifugal Tendency*, due to BSs and UEs close to the boundary of the coverage area, and the distances between the nodes are larger, the average interference will then decrease progressively. Thus, the accuracy of the results provided by IDE becomes lower. However, while the centrifugal tendency is diminishing, CDE yields more accurate results because BSs and UEs close to the center become sparse nodes, which increases the error rate of the measurements.

When the deployment of BSs and UEs tend to *Skewness Tendency*, they gather around a particular area of the network where BSs and UEs are too close to each other. Symmetrically changing the parameters a and b may not provide the same shape variation. Therefore, different observations are made for the values of these two shape parameters. For example, when we increase b, we observe that the accuracy of the results further declines. However, the impact of changing the value of a causes smaller effects over the results. After the value of 10 for a or b, which means higher non-uniform deployments, outcomes of the estimators become less accurate. Especially, the distribution on BSs affects the accuracy of the results significantly in comparison to the distribution of UEs.

With these four deployment tendencies, we also analyze each of BSs and UEs individually such that UEs have a non-uniform tendency, but the distribution of BSs are uniform. In this case, the deployment of UEs follows above three non-uniform tendencies. When UEs have a central tendency, the accuracy of the estimator results is close to each other. However, in the case of centrifugal tendency, IDE and CDE have different accuracy for their outcomes depending on the positions of UEs and BSs in the middle or at the corner, and the inter distances between BSs and UEs. Eventually, when the deployment of BSs and UEs are uniform, if the samples are taken from UEs which are close to the center of the network, two estimators provide more and more accurate results. Furthermore, if the network follows a non-uniform distribution, then the number of the k^{th} nearest neighbor can be increased, and samples can be taken from UEs at anywhere of the environment randomly to get better outcomes. Moreover, we observe that in sparse networks, the performance of IDE is better than CDE because CDE needs collaboration among the UEs in the network. However, in dense networks, CDE gives more accurate results if the samples are collected from UEs randomly for the non-uniform deployments. The average AAPDs of the proposed estimators' results for non-uniform deployments are approximately 27% for IDE and 40% for CDE.

All in all, in Section 3.4, we analyze our proposed estimators by taking into consideration of neighbor proximity, the channel impediments such as shadowing, the impact of the propagation model, and finally we examine the accuracy of the estimators under different non-uniform deployments. We can conclude that RSS-based estimators can be derived by using simple models to ease tractability, but at the same time, we should consider all these factors which are because of the stochastic nature of received signal strength.

4. Density-aware outage analysis

In this section, we demonstrate the impact of density, transmit power and path-loss exponent on network outage [12].

4.1. Simulator model

We uniform randomly determine locations of base stations in a field with an actual deployment density of λ nodes/m^3. A uniform randomly selected point is considered to be the location of the reference user equipment. Using the simple path-loss model described above, we compute the received signal strength from the closest base station. If the signal strength is larger than the threshold value (receiver sensitivity) the run is assumed to be successful; otherwise, an outage occurs. The ratio of outages out of 10^4 runs of the simulations is recorded as the outage probability. We simulated a $500 \times 500 \times 500$ m^3 area, with a transmit power of 100 mW, by considering different deployment densities such as sparse, dense and ultra-dense, and the path-loss exponent is three; i.e., $\gamma = 3$. The values of the parameters employed in the simulations are shown in Table 1. In the figures we present in this section, we show the results of the simulations together with the results of the analytic model in (9).

4.2. Impact of network density on outage

As density increases, there will be a larger number of base stations deployed in the field. Consider a randomly selected user equipment in the field. The distance of it to the closest BS will be smaller; consequently, the path-loss will be smaller in dense networks. As shown in Fig. 7, the outage probability in dense networks will be smaller assuming that all other parameters are kept constant. The density of BSs impacts the quality of service as shown in Fig. 7. The transmit power has a positive impact on the received signal strength. The more transmit power means more receive signal strength as it can be understood from the propagation model and is presented in Fig. 7. When the network is dense, the outage probability will decrease obviously.

For the same distance and level of noise, the crucial factor affecting the quality of communication is the threshold level of sense; i.e., receiver sensitivity. In other words, it is easier to communicate with a UE that has a higher level of sensitivity as demonstrated in Fig. 7. By increasing the complexity of receivers, the threshold can be decreased. Complexity and cost of receivers introduce a trade-off with coverage.

Fig. 7 demonstrates the relation between outage P_O, λ and γ. The path loss exponent (γ) negatively affects the received signal strength. When the channel is prone to high loss, i.e., when the environment is harsh, it is more probable for the randomly selected reference node to be out of coverage.

4.3. Impact of transmit power on outage

A large amount of transmit power is beneficial for the quality of service in a network albeit bad for the environment. The more transmit power implies the more coverage area when the other variables are constant. Furthermore, it implies a larger amount of interference. However, in this paper, we assume a robust interference management scheme that may overcome the negative impact of interference on capacity. If the density of the network increases, e.g., additional (mobile) base stations are deployed or redundant base stations are turned on, the outage probability approaches to zero as shown in Fig. 8. The threshold has the same impact on a network similar to that of the density. If the threshold decreases then the outage approaches to zero (Fig. 8).

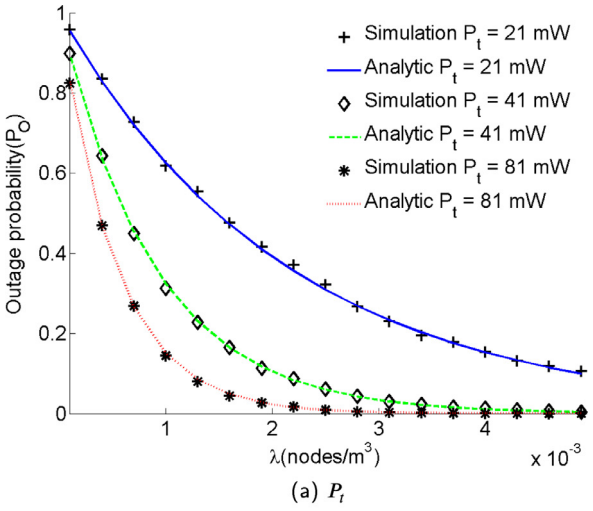

(a) P_t

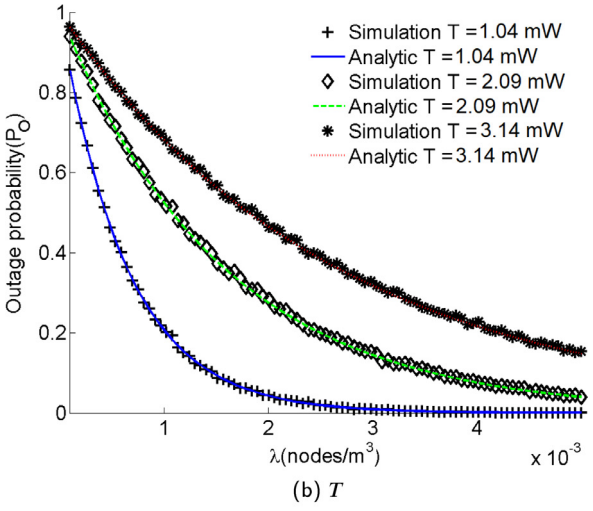

(b) T

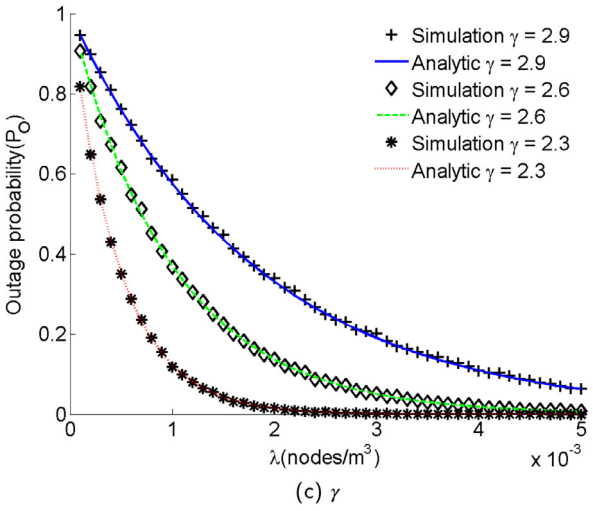

(c) γ

Fig. 7. Impact of density on outage probability for various parameters.

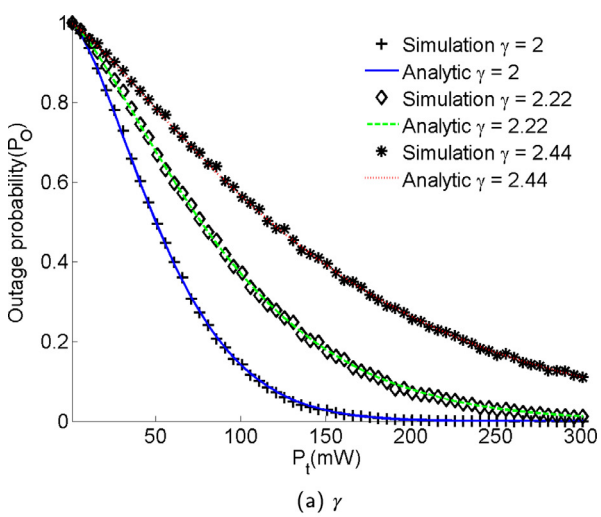

(a) γ

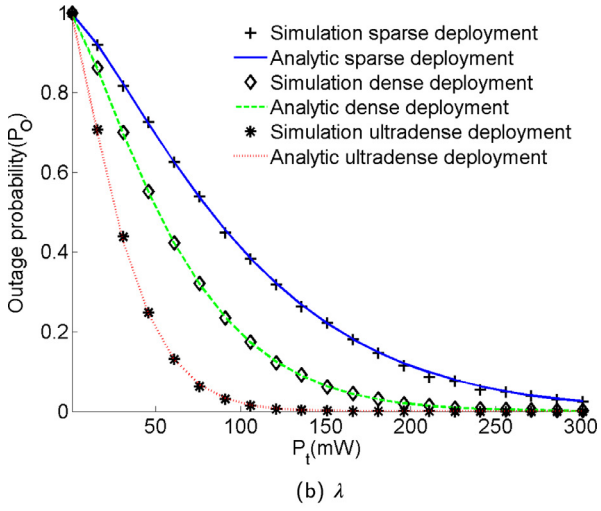

(b) λ

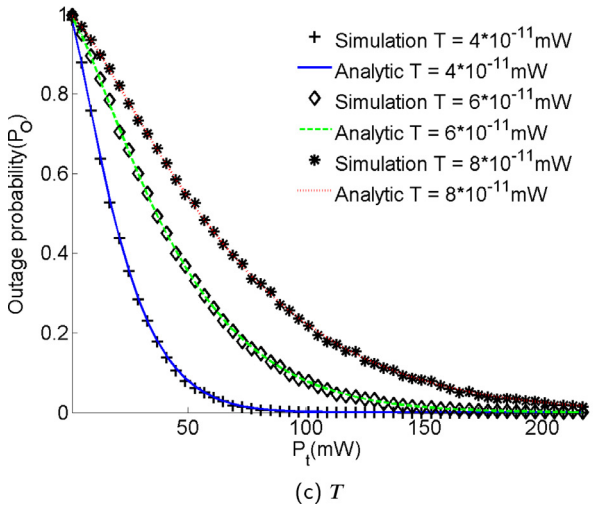

(c) T

Fig. 8. Impact of transmit power on outage probability for various parameters.

4.4. Impact of path-loss exponent on outage

The path loss exponent is a significant factor that characterizes the wireless channel. When γ is extremely high, then it is more probable to be out of coverage as it can be observed in Figs. 8 and 9. Let's consider the same transmit power, it can be clearly seen that when the path-loss exponent is high then the network coverage will decrease. Thus, it is more important that an estimator should determine the channel conditions like the path-loss exponent.

4.5. Impact of receiver sensitivity on outage

We consider the receiver sensitivity as a threshold value that is the minimum requirement to be able to decode signals. If the threshold value increases, the outage probability will increase as it is shown in Fig. 9. Increasing the transmit power leads to a declining outage ratio. As it can be seen in Fig. 9, both the threshold and the path-loss exponent considerably affect the network outage.

5. Validation of density-aware outage probability

In the light of the results presented in Section 4, we claim that in a cellular network, base stations have to change their transmit power according to the network density. The base stations have to be able to estimate the network density by means of equipped with tools and techniques. Pre-configured decisions will not be sufficient since especially when mobile base stations are considered, future cellular networks will be highly dynamic. Statically, configured parameters will decrease the quality of service, and result in many coverage control problems. In this work, we present a run-time adaptable density-aware and -adaptive three-dimensional cell zooming technique using (9), and validate it by using Algorithm 1. For one deployment density (λ) and one transmit power (P_t) settings the time complexity of Algorithm 1 is $O(S)$, where S is the number of simulation runs. This adaptation is also important for energy conservation. After determining the minimum transmit power budget of a base station using this technique, the power can be allocated to individual users or resource blocks [34] as a sequel that is out of the scope of this work.

Algorithm 1 Validation of the Density-aware Outage Probability Model.

Input: λ, γ, P_t, k, T, $Cntr = 0$
Output: (Analytic) P_{O_A} and (Simulated) P_O
for $S = 0$; S<10000; S++ **do**
  Select a set of UE and BSs;
  Find ($\widehat{\lambda}$) by using CDE (8) or IDE (5);
  Select a UE as reference (node);
  Find r_k using Euclidean distances between UE and BSs, where $k = 1$;
  Calculate $x_k \leftarrow CP_t\left(\frac{r_0}{r_k}\right)^{\gamma}$;
  if If $x_k < T$ **then**
    $Cntr$++; //This UE is in outage
  else
    Do nothing; //This UE is in the coverage area
  end if
end for
Find P_{O_A} by using (9) with $\widehat{\lambda}$
$P_O \leftarrow Cntr/S$;
return (P_{O_A}, P_O);

In Algorithm 1, a set of uniform randomly distributed base stations and user equipment with a density of λ (nodes/m^3) is simulated using MATLAB. In a three-dimensional field, after selecting

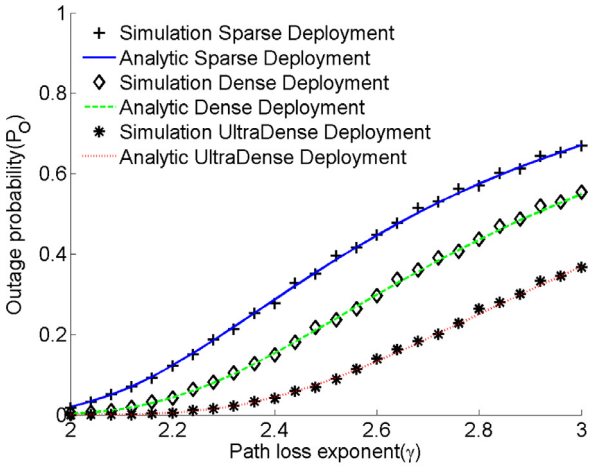

(a) γ

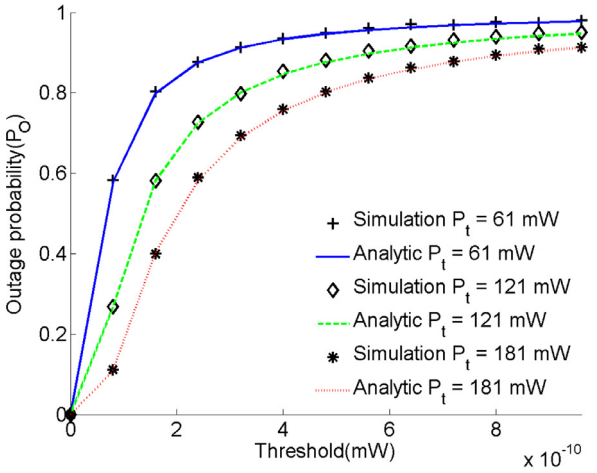

(b) P_t

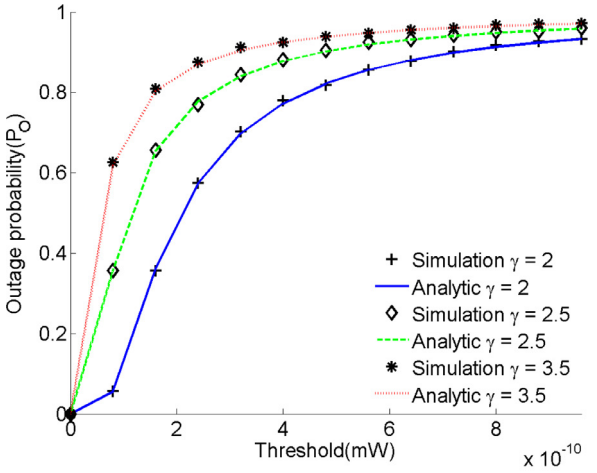

(c) γ

Fig. 9. Impact of path-loss exponent (γ) and threshold (T) on outage probability for various parameters.

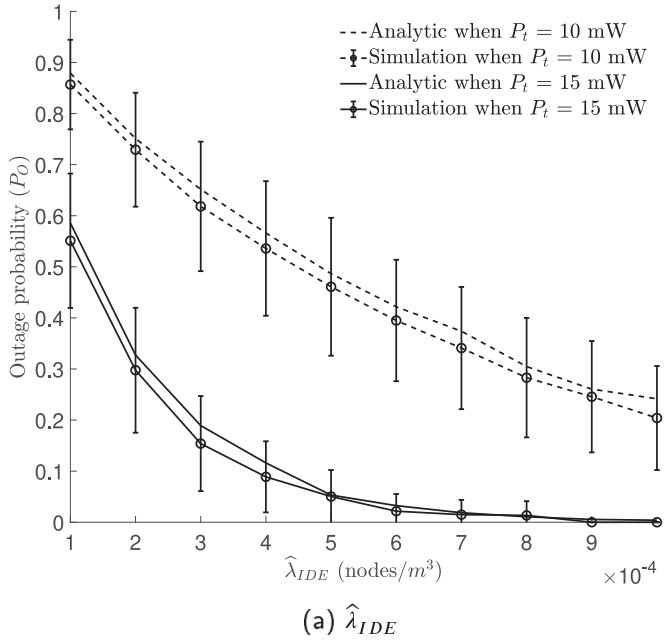

(a) $\widehat{\lambda}_{IDE}$

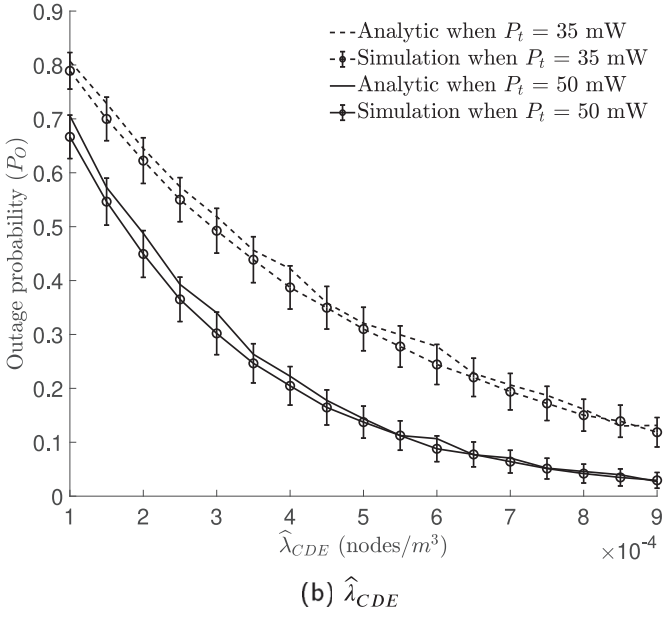

(b) $\widehat{\lambda}_{CDE}$

Fig. 10. Analytic outage values based on the estimated network density $\widehat{\lambda}_{IDE}$ and $\widehat{\lambda}_{CDE}$ for different transmit powers (P_t) when the network density is changing.

a set of base station and user equipment positions, the estimated density ($\widehat{\lambda}$) is calculated. Then, a random point is picked as the position of the reference user equipment (UE). The distance between the UE and the closest base station is found, using the channel model presented in Section 9, and we calculate the received signal strength. If the received signal strength is less than the given threshold (T), this simulation run is recorded as an outage. For the same simulation environment, the simulations are repeated 10^4 times and the ratio of outages is computed. According to the results, we compare the analytic outage probability (P_{O_A}) by considering (9) and the simulated outage ratio (P_O).

In Fig. 10a and b, we show the adapted outage probability for various transmit powers as the density of the network changes. These simulation results validate the analytic model for cell zooming presented in (9) and in (7). The results indicate that if the transmit power of BSs (P_t) does not change, the outage probability (P_O) of a UE decreases when the network is getting denser. However, in sparse networks, the outage probability increases if the same P_t is used. This results also claims that there is a direct relation between the base station density and network outage. By considering the impact of the estimators, it can be said that since CDE is based on collaboration between the nodes, and if the k^{th} nearest neighbor increases, the variance of the results will be smaller than IDE. Depending on the positions of selected UEs and BSs, the accuracy of the results is changing. For instance, UEs and BSs located close to the center of the network increase the accuracy of results, on the other hand, UEs and BSs near to the border of the coverage area decreases the results. When a network operator becomes more tolerant to degraded quality of experience by users due to the outage, the amount of energy conservation can be increased. However, customer satisfaction is significantly related to the outage probability. As the network density increases, it will be required to decrease the transmit power in a density-aware fashion to preserve coverage, to keep the outage probability under control and to conserve energy. The main advantage of the proposed cell zooming technique is that it requires minimal communication overhead, fast and simple to implement. However, the deficiencies of the estimator have to be enhanced. A much faster density estimator that is tolerant to correlated samples is required.

6. Validation of the density-aware power adaptation

In this section, we validate (10) by using two different schemes: one of them is based on the global density of BSs that we used in Section 5, where all measurements are collected with the help of edge computing. As the second approach, each of BSs determines its own density result without using edge computing, in other words, we use local densities belongs to each of BSs.

6.1. Validation of density-aware power adaption technique with edge computing

In order to validate (10), we follow Algorithm 2. The algorithm has O(S) time complexity, where (S) is the simulation count for one deployment density (λ) and one required outage (P_O^*). We simulate a spherical volume consisting of uniform randomly distributed BSs and UEs with different actual deployment densities of λ (nodes/m^3). At each simulator run, we estimate the effective density for the whole network, then we select a random point to be used as the reference UE. We update the transmit power of each BS by considering the model in (10). Then, we calculate the RSS based on the simple path-loss model explained in Section 2.3 from the closest BS of the reference UE where γ is 2. If the computed RSS is lower than the given threshold value T, the result of this run is classified as an outage, otherwise, it is evaluated as successful since it is within the coverage of the clustered network. We run the simulations 10^4 times and the ratio of the number of outages to the total number of simulation runs is determined as outage ratio that is represented as achieved P_O in Table 8 with using $\widehat{\lambda}_{IDE}$, and $\widehat{\lambda}_{CDE}$.

The outage model (9) and the transmit power adaptation technique in (10) provide us accurate results as it can be seen in Table 8. For each required outage value, we use different actual density (λ) values which are between 1×10^{-4} (nodes/m^3) and 9×10^{-4} (nodes/m^3). Then the average outage results for different densities are presented. The achieved outage closely matches the required outage which means that the proposed transmit power adaptation technique based on the provided outage probability is successful. Each of the estimators can be used in order to make the network coverage dynamic. The main conclusion to be drawn

Algorithm 2 Validation of the Density-aware Power Adaptation Technique.

Input: λ, γ, P_t, k, T, P_0^*, $Cntr = 0$
Output: (Simulated) P_0
for $S = 0$; S<10000; S++ **do**
  Select a set of UE and BSs;
  Find $(\widehat{\lambda})$ by using CDE (8) or IDE (5);
  Set P_t^* for all BSs using (10) with $\widehat{\lambda}$ and P_0^*
  Select a UE as reference (node);
  Find r_k using Euclidean distances between UE and BSs, where $k = 1$;
  Calculate $x_k \leftarrow CP_t\left(\frac{r_0}{r_k}\right)^{\gamma}$;
  if If $x_k < T$ **then**
    $Cntr$++; //This UE is in outage
  else
    Do nothing; //This UE is in the coverage area
  end if
end for
$P_0 \leftarrow Cntr/S$;
return (P_0);

is that the relation between the density of base stations and network outage require the adaptation of the transmit power by considering this relation.

6.2. Validation of density estimator and power adaption technique without edge computing

A new approach as utilizing both of these estimators without using the edge computing can be applied locally in the network, and the power adaptation technique can be employed with these local estimation measurements. In other words, instead of the global density of the network, each of the base stations can use its own effective density result.

In these simulations, as it can be seen in Fig. 11 each base station uses its calculated density measurement by using density estimations of its connected closest UEs. Each user equipment receives a number of RSS measurements from their first k closest base stations and estimates the density by employing the IDE or the CDE methods. Each base station collects the estimation results from their closest user equipment, and the average of these estimations are calculated as local base station density. After each base station determines the density result itself, (10) is used for adapting the transmit power based on the required outage probability. In the simulations, the same approach like in Section 6 is exploited so that every time each BS changes its transmit power based on the estimated density and the outage probability.

Table 9 presents the AAPD results between the required outage and the analytic outage values. The average outage results for different densities are presented. In these simulations, at each run of the simulation, each BS calculates its own density instead of using the global density, then they change their transmit powers using the model in (10). For the rest of the steps, the same approach in Section 5 is used for calculating the required outage and analytic outage. The results in Tables 8 and 9 indicate that IDE has more accurate results so that we may employ IDE as a density estimator based on the measurements of its associated UEs. Since CDE needs more measurements than IDE, it provides less accurate results in comparison to the outcomes of IDE. In these simulations, more accurate results are obtained while the large number of UE is considered and the network is getting denser.

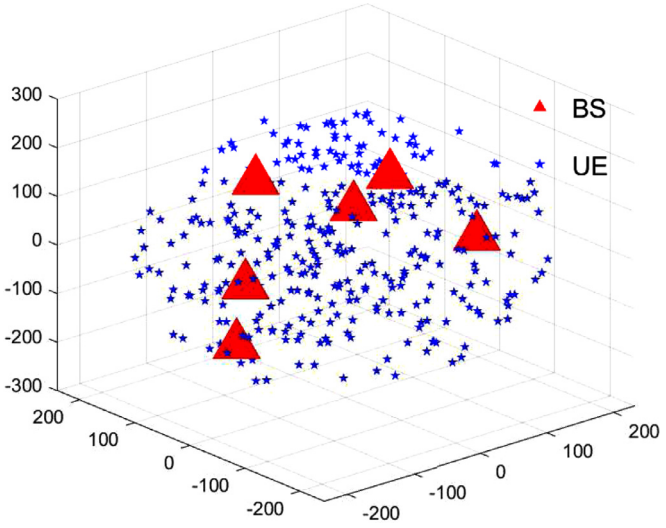

Fig. 11. Collecting $\widehat{\lambda}$ measurements (nodes/m^3) from the first k nearest UEs.

7. Related work

In this section, we present the related work in a categorized fashion.

7.1. Distribution of base stations

In cellular networks, the spatial distribution of base stations in order to obtain optimal deployments has been coming into prominence. The stochastic models including optimum base station density have paramount importance to analyze the network performance in terms of coverage, energy efficiency and quality of service [35,36]. With the improvement of the network, to provide higher capacity and coverage to users, increasing the number of base stations is considered as a handy solution which is called densification. Moreover, with the proliferation of base stations on wheels and wings, small cells, and the user-controlled base stations always result in topology changes in the network. In that sense, analyzing the spatial distribution of base stations by using the theoretical models is always a principal topic in wireless

Table 8
Required outage probability (P_0^*) vs calculated outage probability (P_0) by using the $\widehat{\lambda}_{IDE}$, $\widehat{\lambda}_{CDE}$, which are the global density of base stations, and AAPD (%) results.

P_0^*	$\widehat{\lambda}_{IDE}$			$\widehat{\lambda}_{CDE}$		
	P_0	AAPD, %	99% confidence limits, ($\times 10^{-5}$)	P_0	AAPD, %	99% confidence limits, ($\times 10^{-5}$)
0.02	0.022	11.31	±1.12	0.022	8.81	±0.28
0.025	0.027	6.93	±1.13	0.027	7.29	±0.36
0.03	0.031	4.37	±1.35	0.031	4.71	±0.33
0.035	0.036	2.92	±0.96	0.036	4.06	±0.36
0.04	0.040	1.14	±1.38	0.041	3.60	±0.27
0.045	0.045	0.54	±1.23	0.046	2.35	±0.19

Table 9
Required outage probability (P_O^*) vs calculated outage probability (P_O) by using the $\widehat{\lambda}_{IDE}$ (nodes/m^3), $\widehat{\lambda}_{CDE}$ (nodes/m^3), which are the local density results belong to each of BSs, and AAPD (%) results.

P_O^*	$\widehat{\lambda}_{IDE}$			$\widehat{\lambda}_{CDE}$		
	P_O	AAPD, %	99% confidence limits, ($\times 10^{-5}$)	P_O	AAPD, %	99% confidence limits, ($\times 10^{-5}$)
0.02	0.022	8.46	$\pm$0.98	0.023	17.60	$\pm$0.52
0.025	0.027	7.26	$\pm$2.35	0.029	15.00	$\pm$1.68
0.03	0.031	4.69	$\pm$2.07	0.034	12.84	$\pm$1.10
0.035	0.036	2.72	$\pm$1.45	0.039	12.17	$\pm$0.95
0.04	0.041	1.38	$\pm$2.48	0.044	7.61	$\pm$1.13
0.045	0.045	0.84	$\pm$2.74	0.049	7.28	$\pm$2.93

networks and still an open research question for next-generation networks [37]. Although there are different statistical distributions models such as Poisson, lognormal, Weibull, generalized Pareto and alpha-stable in order to model the base station spatial density, most of the studies leverage Poisson due to tractability as stated in [37]. In addition to the base station density, the recent studies reveal that the stochastic models including PPP provide tractable models to control the cell size by considering the coverage probability and adaptation of transmit power [35,38,39]. In order to provide an enhanced quality of service mobile base stations and drone base stations can be used as fast deployments, however, these networks require to transmit power adaptation in terms of energy efficiency, trajectory plans, and user connectivity [40–42]. Transmit power can be minimized by increasing the number of base stations until the network density reaches a threshold value. The optimal network density provides an optimum power consumption and enhanced coverage as stated in [43].

7.2. Existing density estimation methods

Since future cellular networks has a dynamic topology, the need for the existence of robust density estimators is an open issue. Existing density estimators can be classified as (1) location-based; (2) neighbor discovery based, and (3) received signal strength (RSS) based methods. Location-based methods rely on GPS; e.g., node census (NC) [44]. Auxiliary systems consume extra energy, and the density estimate is subject to localization errors. Neighborhood discovery based methods estimate density based on inferences drawn from in-network communication; e.g., NEST [45]. The accuracy depends on the traffic amount. The RSS-based density estimators are proposed in [18,19] for two-dimensional ad-hoc networks. This type combines the merits of location-based and neighbor discovery based estimation and overcomes their drawbacks. However, the time required to compute the estimator may be long.

7.3. How density of base stations affects network coverage and capacity

Ultra-dense networks (UDN) are expected to provide high capacity. The potential of higher frequency bands is analyzed in [46]. In that work, UE and BS density, UE distribution and energy efficiency in a network are used to calculate transmit power by considering signal-to-interference-plus-noise ratio (SINR) for providing better coverage. In a mobile network consisting of a large number of uniform randomly deployed BSs, the outage probability decreases with an increasing ratio of mobile-to-BS density [47]. An interference model for wireless networks consisting of uniform randomly distributed nodes is combined with different types of popular fading models in [48]. This model considers the interference power by using a partial cancellation method and outage probability calculated by using the nearest interferer instead of the total interference power since the nearest interferer dominates the total interference. A stationary receiver is considered as a base station for a given user and the same transmit power is considered for mobile units.

In the case of 5G networks, connectivity and coverage are two important optimization parameters related to each other, and designers should consider them jointly as in ad hoc networks [49,50]. It is underlined that the connectivity problem may not be handled without adapting the transmit power to the network via presenting the results with two-dimensional simulations and models applying the connectivity of nodes, transmit power and density for an ad hoc network. As the dynamic and distributed nature of the future networks' architecture, mobile ad hoc networks (MANET) have a distributed and self-organized structure [51]. One of the sample applications of MANETs is the vehicular ad hoc networks (VANETs). [52] states that such networks have a dynamic structure that necessitates adapting the transmit power to some parameters network such as distance between mobile nodes, density, the antenna type and type of broadcasting for enhancing network performance. Density and distance are the selected parameters for adapting transmit power in [52]. Density refers to the number of nodes in a network per unit area. In dense networks, the distance among nodes will be shorter. On the other hand, the distances among nodes will be larger when the network is sparse. Hence, if the network is sparse, the transmit power should be increased based on the distance between the nodes, but if the network is dense then we need less transmit power since the distance between nodes will be smaller. However, we should consider the outage and the interference in the network [5,53]. When the network is sparse, the probability of outage will be higher and when the network is dense then the interference between nodes will be higher if the transmit power is not adapted to these changes.

7.4. Relation between aggregate interference, path-loss and BS density

Understanding the characterization of aggregate interference power in terms of the base station deployment and interference management can provide better performance for homogeneous and heterogeneous networks [54]. Joint power control and user scheduling are proposed for ultra-dense networks by considering dynamic channel conditions and unknown traffic demands in [55]. The aim of this model is to ensure energy efficiency while supplying the quality of service and reducing the number of UEs in outage depending on queue capacities of BSs. The network outage is considered the fraction of undesired UEs whose handovers cannot be admitted because of the queue capacity limitations, and the density is determined as the average inter-site distance (ISD) for a large homogeneous UDN deployment. In addition to homogeneous cellular networks, a heterogeneous network is considered, and a model consisting of optimal BS density by conceiving the QoS limitations is analyzed in [56]. The proposed model aims at making the network energy efficient and analyzes the effect of network density on cost. A threshold value obtained by using path-loss and

transmit power of the relevant BS is used to define outage probability.

With the proliferation of small cells, the fractal characteristic of the coverage for cellular networks is more prone to the path-loss effects [31,57,58]. In small cells, the characterization of wireless propagation environment is volatile and complicated as stated in [31] on the occasion of not only regular but also non-uniform obstructions arising from buildings, infrastructures, tress, and erratic weather conditions. Both the line-of-sight and non-line-of-sight signals affect the path-loss exponent value or path-loss coefficient. Two different path-loss models are introduced, which are isotropic and anisotropic by considering propagation directions. Isotropic models are commonly used in the literature to make models simple as much as possible. However, due to the fractal characteristics of cellular networks, the anisotropic models can be leveraged to make network models more realistic [57]. In our study, we exploit a simple path-loss model which is simplified from Winner II channel models to propose simple and easily tractable models [24]. This model has already been analyzed in [18], and it is illustrated that the RSS-based approaches including simple path-loss model may be used for real-life experiments with 10 percentage error rate.

In this study, unlike the existing works firstly we propose two novel base station density estimators, the interference-based density estimation and multi-access edge cloud-based estimation based on received signal strength, which are operational in a three-dimensional environment. Secondly, two proposed models to control the network outage and cell size are simple and compact solutions. Finally, we present a qualitative and elaborated analysis of different network parameters at the same time depends on the network density. The proposed approaches leverage a three-dimensional PPP distribution which provides easily understandable and tractable models.

8. Conclusion

With the invention of mobile devices, applications, and new network paradigms such as ultra-dense networking, mobile cells, ever-changing topologies, the need for self-organized networking becomes more pronounced in order to increase the capacity, coverage, and performance. Dense networks provide redundant coverage whereas connectivity is disrupted in sparse networks. In this paper, we propose novel network density estimators based on received signal strength. One of them uses the aggregated measurements (IDE) and the other one exploits the collaboratively collected measurements (CDE). We propose the system design for density estimation in mobile networks and validate the proposed estimators using Monte-Carlo simulations implemented in Matlab. We presented three significant outcomes in this paper. First of all, two robust density estimators are proposed and validated. Secondly, a simple outage probability model is proposed and validated. As the last contribution, we propose a density-aware transmit power adaptation technique in a dynamic and self-configurable fashion for conserving energy and enhancing the quality of service. From a theoretic perspective, models consider only large-scale fading and is applicable in environments where the impact of shadowing is small. As future work, we will implement estimators in outdoor and indoor test-beds and validate the results in practice. We will also incorporate shadowing in the estimator. According to the results, transmit power of base stations must be density-aware to increase the network capacity. We analyzed the impact of transmit power, channel model and density on outage probability. As expected transmit power and network density are quality of service-friendly parameters, unlike the rest. However, they are not cost- or environment-friendly.

Declaration of competing Interest

The authors declare that they have no known competing financial interests or personal relationships that could have appeared to influence the work reported in this paper.

Acknowledgements

This work was supported by TÜBİTAK, Project 215E127.

Supplementary material

Supplementary material associated with this article can be found, in the online version, at doi:10.1016/j.comnet.2019.106922.

References

[1] I. Bor-Yaliniz, H. Yanikomeroglu, The new frontier in RAN heterogeneity: multi-tier drone-cells, IEEE Commun. Mag. 54 (11) (2016) 48–55.
[2] M. Kamel, W. Hamouda, A. Youssef, Ultra-dense networks: a survey, IEEE Commun. Surv. Tutor. 18 (4) (2016) 2522–2545, doi:10.1109/COMST.2016.2571730.
[3] C. Galiotto, N.K. Pratas, L. Doyle, N. Marchetti, Effect of LOS/NLOS propagation on 5G ultra-dense networks, Comput. Netw. 120 (2017) 126–140, doi:10.1016/j.comnet.2017.04.012.
[4] S. Sharafeddine, R. Islambouli, On-demand deployment of multiple aerial base stations for traffic offloading and network recovery, Comput. Netw. 156 (2019) 52–61, doi:10.1016/j.comnet.2019.03.016.
[5] Q.-T. Thieu, H.-Y. Hsieh, Outage protection for cellular-mode users in device-to-device communications through stochastic optimization, Comput. Netw. 132 (2018) 145–160, doi:10.1016/j.comnet.2018.01.006.
[6] H. Wang, G. Ren, J. Chen, G. Ding, Y. Yang, Unmanned aerial vehicle-aided communications: joint transmit power and trajectory optimization, IEEE Wirel. Commun. Lett. 7 (4) (2018) 522–525, doi:10.1109/LWC.2018.2792435.
[7] T. Zahir, K. Arshad, A. Nakata, K. Moessner, Interference management in femtocells, IEEE Commun. Surv. Tutor. 15 (1) (2013) 293–311, doi:10.1109/SURV.2012.020212.00101.
[8] B. Rengarajan, G. Rizzo, M.A. Marsan, Energy-optimal base station density in cellular access networks with sleep modes, Comput. Netw. 78 (2015) 152–163, doi:10.1016/j.comnet.2014.10.032. Special Issue: Green Communications.
[9] L. SuÁrez, L. Nuaymi, J.-M. Bonnin, Energy-efficient bs switching-off and cell topology management for macro/femto environments, Computer Networks 78 (2015) 182–201, doi:10.1016/j.comnet.2014.10.028. Special Issue: Green Communications.
[10] Y.-C. Wang, C.-A. Chuang, Efficient ENB deployment strategy for heterogeneous cells in 4G lte systems, Comput. Netw. 79 (2015) 297–312, doi:10.1016/j.comnet.2015.01.013.
[11] D. Han, H. Minn, U. Tefek, T.J. Lim, Network dimensioning, QOE maximization, and power control for multi-tier machine-type communications, IEEE Trans. Commun. 67 (1) (2019) 859–872, doi:10.1109/TCOMM.2018.2875735.
[12] O. Yaman, A. Eroglu, E. Onur, Density-aware cell zooming, in: 2018 21st Conference on Innovation in Clouds, Internet and Networks and Workshops (ICIN), 2018, pp. 1–8, doi:10.1109/ICIN.2018.8401612.
[13] S. Jagadeesan, J. Riihijirvi, M. Petrova, Impact of three-dimensionality of femtocell deployments on aggregate interference estimation, in: 2015 IEEE 26th Annual International Symposium on Personal, Indoor, and Mobile Radio Communications (PIMRC), 2015, pp. 737–742, doi:10.1109/PIMRC.2015.7343395.
[14] Z. Niu, Y. Wu, J. Gong, Z. Yang, Cell zooming for cost-efficient green cellular networks, IEEE Commun. Mag. 48 (11) (2010) 74–79, doi:10.1109/MCOM.2010.5621970.
[15] H. Chen, Q. Zhang, F. Zhao, Energy-efficient joint BS and RS sleep scheduling in relay-assisted cellular networks, Comput. Netw. 100 (2016) 45–54, doi:10.1016/j.comnet.2016.02.016.
[16] R. Balasubramaniam, S. Nagaraj, M. Sarkar, C. Paolini, P. Khaitan, Cell zooming for power efficient base station operation, in: Proc. of the 9th IWCMC, 2013, pp. 556–560, doi:10.1109/IWCMC.2013.6583618.
[17] S. Manegene, S. Musyoki, P. Langat, Application of cell zooming in outage compensation, J. Electron. Commun.Eng. 10 (4) (2015) 60–69.
[18] A. Eroglu, E. Onur, H. Oguztuzun, Estimating density of wireless networks in practice, in: Proc. of the PIMRC, 2015, pp. 1476–1480, doi:10.1109/PIMRC.2015.7343531.
[19] E. Onur, Y. Durmus, I. Niemegeers, Cooperative density estimation in random wireless ad hoc networks, IEEE Commun. Lett. 16 (3) (2012) 331–333.
[20] M. Haenggi, Efficient routing in wireless networks with random node distribution, in: International Symposium on Information Theory, 2004. ISIT 2004. Proceedings., 2004, p. 17, doi:10.1109/ISIT.2004.1365056.
[21] D. Moltchanov, Distance distributions in random networks, Ad Hoc Netw. 10 (6) (2012) 1146–1166 https://doi.org/10.1016/j.adhoc.2012.02.005.
[22] M. Haenggi, On distances in uniformly random networks, IEEE Trans. Inf. Theory 51 (10) (2005) 3584–3586, doi:10.1109/TIT.2005.855610.
[23] W.J. Cody, An overview of software development for special functions, in: G.A. Watson (Ed.), Numerical Analysis, Springer, Berlin, Heidelberg, 1976, pp. 38–48.

[24] P. Kyösti, J. Meinilä, L. Hentila, X. Zhao, T. Jämsä, C. Schneider, M. Narandzi'c, M. Milojevi'c, A. Hong, J. Ylitalo, V.-M. Holappa, M. Alatossava, R. Bultitude, Y. Jong, T. Rautiainen, Ist-4-027756 WINNER II d1.1.2 v1.2 WINNER II channel models, Inf. Soc. Technol. 11 (2008).
[25] Z. Liu, F. Li, Y. Qi, J. Chen, An effective receiver sensitivity measurement, in: 2015 IEEE Symposium on Electromagnetic Compatibility and Signal Integrity, 2015, pp. 310–313, doi:10.1109/EMCSI.2015.7107705.
[26] A. Eroglu, E. Onur, M. Turan, Density-aware outage in clustered ad hoc networks, in: 2018 9th IFIP International Conference on New Technologies, Mobility and Security (NTMS), 2018, pp. 1–5, doi:10.1109/NTMS.2018.8328688.
[27] S. Mollahasani, E. Onur, Density-aware, energy- and spectrum-efficient small cell scheduling, IEEE Access 7 (2019) 65852–65869, doi:10.1109/ACCESS.2019.2917722.
[28] T. Rappaport, Wireless Communications: Principles and Practice, second ed., Prentice Hall PTR, Upper Saddle River, NJ, USA, 2001.
[29] G. Mao, B. Fidan, B.D. Anderson, Wireless sensor network localization techniques, Comput. Netw. 51 (10) (2007) 2529–2553, doi:10.1016/j.comnet.2006.11.018.
[30] S.D. Chitte, S. Dasgupta, Z. Ding, Distance estimation from received signal strength under log-normal shadowing: bias and variance, in: 2008 9th International Conference on Signal Processing, 2008, pp. 256–259.
[31] X. Ge, X. Tian, Y. Qiu, G. Mao, T. Han, Small-cell networks with fractal coverage characteristics, IEEE Trans. Commun. 66 (11) (2018) 5457–5469, doi:10.1109/TCOMM.2018.2849391.
[32] V.I. Ogurtsov, D.B. Papkovsky, Modeling of luminescence-based oxygen sensors with non-uniform distribution of excitation and quenching characteristics inside active medium, Sens. Actuators B 88 (1) (2003) 89–100, doi:10.1016/S0925-4005(02)00312-X.
[33] A.K. Gupta, S. Nadarajah, Handbook of Beta Distribution and its Applications, CRC press, 2004.
[34] C.S. Chen, F. Baccelli, Self-optimization in mobile cellular networks: power control and user association, in: Proc. of the IEEE International Conference on Communications, 2010, pp. 1–6.
[35] S. Chatterjee, M.J. Abdel-Rahman, A.B. MacKenzie, Optimal base station deployment with downlink rate coverage probability constraint, IEEE Wirel. Commun. Lett. 7 (3) (2018) 340–343, doi:10.1109/LWC.2017.2776929.
[36] T. Zhang, J. Zhao, L. An, D. Liu, Energy efficiency of base station deployment in ultra dense hetnets: a stochastic geometry analysis, IEEE Wirel. Commun. Lett. 5 (2) (2016) 184–187, doi:10.1109/LWC.2016.2516010.
[37] L. Chiaraviglio, F. Cuomo, M. Maisto, A. Gigli, J. Lorincz, Y. Zhou, Z. Zhao, C. Qi, H. Zhang, What is the best spatial distribution to model base station density? A deep dive into two european mobile networks, IEEE Access 4 (2016) 1434–1443, doi:10.1109/ACCESS.2016.2552981.
[38] M. Di Renzo, T.T. Lam, A. Zappone, M. Debbah, A tractable closed-form expression of the coverage probability in poisson cellular networks, IEEE Wirel. Commun. Lett. 8 (1) (2019) 249–252, doi:10.1109/LWC.2018.2868753.
[39] G. George, A. Lozano, M. Haenggi, Distribution of the number of users per base station in cellular networks, IEEE Wirel. Commun. Lett. (2018) 1, doi:10.1109/LWC.2018.2878579.
[40] S.A. Hadiwardoyo, E. Hernández-Orallo, C.T. Calafate, J.C. Cano, P. Manzoni, Experimental characterization of UAV-to-CAR communications, Comput. Netw. 136 (2018) 105–118, doi:10.1016/j.comnet.2018.03.002.
[41] H. Sallouha, M.M. Azari, A. Chiumento, S. Pollin, Aerial anchors positioning for reliable RSS-based outdoor localization in urban environments, IEEE Wirel. Commun. Lett. 7 (3) (2018) 376–379, doi:10.1109/LWC.2017.2778723.
[42] L. Wang, B. Hu, S. Chen, Energy efficient placement of a drone base station for minimum required transmit power, IEEE Wirel. Commun. Lett. (2018) 1, doi:10.1109/LWC.2018.2808957.
[43] S. Sarkar, R.K. Ganti, M. Haenggi, Optimal base station density for power efficiency in cellular networks, in: 2014 IEEE International Conference on Communications (ICC), 2014, pp. 4054–4059, doi:10.1109/ICC.2014.6883955.
[44] M.H. Raza, L. Hughes, I. Raza, Density: a context parameter of ad hoc networks, in: O. Castillo, L. Xu, S.-I. Ao (Eds.), Trends in Intelligent Systems and Computer Engineering, Lecture Notes in Electrical Engineering, 6, Springer US, 2008, pp. 525–540.
[45] V. Iyer, A. Loukas, S. Dulman, Nest: A Practical Algorithm for Neighborhood Discovery in Dynamic Wireless Networks using Adaptive Beaconing, Technical Report, Delft University of Technology, 2012.
[46] D. López-Pórez, M. Ding, H. Claussen, A.H. Jafari, Towards 1 Gbps/UE in cellular systems: understanding ultra-dense small cell deployments, IEEE Commun. Surv. Tutor. 17 (4) (2015) 2078–2101, doi:10.1109/COMST.2015.2439636.
[47] S. Lee, K. Huang, Coverage and economy of cellular networks with many base stations, IEEE Commun. Lett. (2012) 1038–1040.
[48] V. Mordachev, S. Loyka, On node density - outage probability tradeoff in wireless networks, in: Proc. of the IEEE International Symposium on Information Theory, 2008, pp. 191–195, doi:10.1109/ISIT.2008.4594974.
[49] D. Miorandi, E. Altman, Coverage and connectivity of ad hoc networks presence of channel randomness, in: Proc. of the IEEE Annual Joint Conf. of the IEEE Computer and Communications Societies., 2005, pp. 491–502 vol. 1, doi:10.1109/INFCOM.2005.1497917.
[50] N. Panwar, S. Sharma, A.K. Singh, A survey on 5G: the next generation of mobile communication, Phys. Commun. 18 (2016) 64–84.
[51] A. Madhja, S. Nikoletseas, A.A. Voudouris, Adaptive wireless power transfer in mobile ad hoc networks, Comput. Netw. 152 (2019) 87–97, doi:10.1016/j.comnet.2019.02.004.
[52] M.I. Khan, Network parameters impact on dynamic transmission power control in vehicular ad hoc networks, CoRR (2013). abs/1310.4475.
[53] J. Yao, W. Lou, C. Yang, K. Wu, Efficient interference-aware power control for wireless networks, Comput. Netw. 136 (2018) 68–79, doi:10.1016/j.comnet.2018.02.017.
[54] T. Zhang, L. An, Y. Chen, K.K. Chai, Aggregate interference statistical modeling and user outage analysis of heterogeneous cellular networks, in: 2014 IEEE International Conference on Communications (ICC), 2014, pp. 1260–1265, doi:10.1109/ICC.2014.6883494.
[55] S. Samarakoon, M. Bennis, W. Saad, M. Debbah, M. Latva-aho, Ultra dense small cell networks: turning density into energy efficiency, IEEE J. Sel. Areas Commun. 34 (5) (2016) 1267–1280, doi:10.1109/JSAC.2016.2545539.
[56] D. Cao, S. Zhou, Z. Niu, Optimal base station density for energy-efficient heterogeneous cellular networks, in: Proc. of the IEEE ICC, 2012, pp. 4379–4383, doi:10.1109/ICC.2012.6364656.
[57] J. Chen, X. Ge, Q. Ni, Coverage and handoff analysis of 5g fractal small cell networks, IEEE Trans. Wirel. Commun. 18 (2019) 1263–1276.
[58] X. Ge, Y. Qiu, J. Chen, M. Huang, H. Xu, J. Xu, W. Zhang, Y. Yang, C. Wang, J. Thompson, Wireless fractal cellular networks, IEEE Wirel. Commun. 23 (5) (2016) 110–119, doi:10.1109/MWC.2016.7721749.

Alperen Eroğlu received his B.Sc. degree at the department of electronics and computer education as the valedictorian of the department from Firat University, Elazığ, Turkey in 2009, and the M.Sc. degree in computer engineering from METU, Ankara, Turkey in 2015. During the M.Sc., he researched and studied in the fields of robotics, artificial intelligence, software engineering, system architecture and modeling, embedded systems, wireless sensor networks, computer networks. He accomplished his M.Sc. studies in the field of wireless sensor networks. He is currently a Ph.D. student in the department of computer engineering at METU. He has been working as a research and teaching assistant at METU. His research interests are in the area of 5G mobile networks, Internet of Things, computer and wireless networks. He is a member of the Wireless Systems, Networks and Cybersecurity Laboratory (WINSLab). He is a member of IEEE.

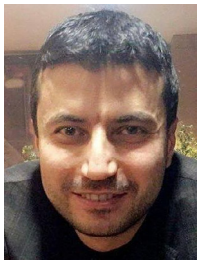

Okan Yaman received his B.Sc. degree in mathematics from METU, Ankara, Turkey in 2012, and the M.Sc. degree in computer engineering from METU in 2016. During the M.Sc., he researched and studied in the fields of machine learning, statistics, mathematical modeling, wireless and computer networks, and their security. He accomplished his M.Sc. studies in the field of wireless networks. After the M.Sc., he worked as the transport network modeler in Turkish National Transport Master Plan funded by the European Union. He is currently pursuing the Ph.D. degree in computer engineering at Izmir Institute of Technology, Izmir, Turkey and YOK doctoral scholar in Sensor Technologies. His research interests are in the computer and wireless networks and their security. He is a member of IEEE.

Ertan Onur received his B.Sc. degree in computer engineering from Ege University, Izmir, Turkey in 1997, and the M.Sc. and Ph.D. degrees in computer engineering from Bogazici University, Istanbul, Turkey in 2001 and 2007, respectively. During the M.Sc. and Ph.D. degrees, he worked as a project leader at Global Bilgi, Istanbul and as an R&D project manager at Argela Technologies, Istanbul. He developed and managed many commercial telecommunications applications. After obtaining his Ph.D. degree, he worked as an assistant professor at Delft University of Technology, the Netherlands. From 2014 on, he is with METU, Turkey. He was the editor/convenor of the Personal Networks Group of Ecma International Standardization Body. Dr. Onur's research interests are in the area of computer and wireless networks and their security. He is the founder of the Wireless systems, Networks and Cybersecurity Laboratory (WINSLab). He is a member of IEEE.